

CHARACTERIZING CREATININE MIP FUNCTIONALITY USING SPECTROSCOPY TECHNIQUES

Bradley Hovan

Submitted in Partial Fulfillment of the Requirements
for the degree of

MASTER OF SCIENCE

Approved by:
Rahmi Ozisik, Chair
Ganpati Ramanath
Edward Palermo



Department of Materials Engineering
Rensselaer Polytechnic Institute
Troy, New York

[December 2021]
Submitted November 2021

© Copyright 2021

By

Bradley Hovan

All Rights Reserved

CONTENTS

LIST OF TABLES.....	v
LIST OF FIGURES.....	vi
ACKNOWLEDGEMENT.....	ix
ABSTRACT.....	x
1 Introduction.....	1
2 Motivation.....	4
2.1 Global Healthcare Standards.....	4
2.1.1 Kidney Disease.....	5
2.1.2 Quantifying Kidney Function: Creatinine.....	6
2.1.3 Diagnostic History: The Jaffe Method.....	8
2.2 Molecular Sensing.....	9
2.2.1 Today's Golden Standard.....	10
2.2.2 Creatinine's Future.....	14
3 Theory.....	16
3.1 Synthetic Receptors – MIPs.....	16
3.1.1 MIPs: How Do They Work?.....	17
3.1.2 MIPS – Key Specifications.....	19
3.1.3 MIP Functional Properties.....	21
3.1.4 Precipitation Polymerization of MIPs.....	23
3.2 Miura et al.'s Creatinine MIP.....	24
3.3 Sensing Creatinine In Solution.....	27
3.4 Scatchard Analysis.....	30
4 Experimental setup.....	32
4.1 Polymer Solvent Preparation.....	32
4.2 Synthesis Apparatus.....	33
4.3 UV-VIS Setup.....	35
5 Experimental plan.....	37
5.1 Polymer Synthesis.....	37
5.1.1 Notes on polymer synthesis.....	39
5.2 Polymer Purification.....	40
5.3 Reference Curve.....	42

5.4	Scatchard Analysis.....	44
5.4.1	Refined Scatchard Analysis	47
6	Results and Discussion: Reference Curve	49
6.1	Reference Curve Experimentation.....	49
6.2	Reference Curve Finalization	53
7	Results and Discussion: Polymer Characterization	57
7.1	Raman Spectra	57
7.2	SEM Images.....	59
8	Results and Discussion: Scatchard Analysis	63
9	Conclusion and Future Work	65
10	References	67
	APPENDIX A: NIR Spectroscopy Data.....	71
	APPENDIX B: Dilution Scheme MATLAB Code.....	73
	APPENDIX C: Reference Curve MATLAB Code	75
	Appendix D: Raman Spectra MATLAB Code.....	79
	APPENDIX E: Scatchard Analysis MATLAB Code	80
	APPENDIX F: Supplementary Files	83

LIST OF TABLES

Table 2-1. Typical pros and cons of enzyme-based molecular sensors.	13
Table 3-1. Each compound in the creatinine MIP detailed by Miura et al.	25
Table 5-1. Reagents used to synthesize the MIP and NIP.....	38

LIST OF FIGURES

Figure 1-1. Kidney transplant statistics [4].	2
Figure 2-1. (left) Basic anatomy of a human kidney [10]. (right) Flow geometries of the kidney demonstrated as the flow within one nephron. " C_{Crea} " is the concentration of creatinine in the respective vessel, demonstrating how creatinine is freely filtered by glomeruli and not effected by the reabsorption mechanisms present for moving fluid/solutes from the tubules (yellow) back into the renal vasculature (red/blue).	7
Figure 2-2. Creatinine and five molecularly-similar compounds found in bodily fluid [6]. Reprinted from Pharmaceutical and Biomedical Analysis, Vol 85, Chitose Miura, Noriko Funaya, Hisami Matsunaga, Jun Haginaka, Monodisperse, molecularly imprinted polymers for creatinine by modified precipitation polymerization and their applications to creatinine assays for human serum and urine, 288-294, 2013, with permission from Elsevier.	8
Figure 2-3. Jaffe method principle reactions. Top displays reactants: creatinine and picric acid. Bottom displays the two forms of the complex resulting from the spontaneous reaction of the reactants, and their respective detectable wavelengths [13].	9
Figure 2-4. (left) Example of an antibody containing an antigen binding site for the reciprocal antigen (in yellow). (right) Simulated protein structure of an antibody, demonstrating how the folding of different protein chains to form one larger unit [16].	11
Figure 2-5. Principle function diagram provided by LSBio for their creatinine ELISA kit, see above text for details [17].	12
Figure 2-6. (a) Structure of iohexol, and (b) structure of inulin. Inulin containing repeating carbohydrate units [19] [20].	14
Figure 3-1. Number of publications with respect to time for MIP biosensors, MIPs, and biosensors, respectively [21]. Reprinted (adapted) from J. Belbruno, "Molecularly Imprinted Polymers," Chemical Reviews, vol. 199, no. 1, pp. 94-119, 2018.. Copyright 2021 American Chemical Society.	16
Figure 3-2. Principle steps for MIP synthesis and function. See text for details [21]. Reprinted (adapted) from J. Belbruno, "Molecularly Imprinted Polymers," Chemical Reviews, vol. 199, no. 1, pp. 94-119, 2018.. Copyright 2021 American Chemical Society.	18
Figure 3-3. Examples of the numerous, imprintable templates for MIPs [23]. Reprinted from BioTechniques, Vol 69, Zahra El-Schich, Yuecheng Zhang, Marek Feith, Sarah Beyer, Louise Sternbæk, Lars Ohlsson, Maria Stollenwerk and Anette Gjorloff Wingren Molecularly imprinted polymers in biological applications, 407–419, 2020, with permission from Creative Commons.	20
Figure 3-4. Imprinting factors for creatinine MIP against five structurally-similar compounds [6]. Reprinted from Pharmaceutical and Biomedical Analysis, Vol 85, Chitose Miura, Noriko Funaya, Hisami Matsunaga, Jun Haginaka, Monodisperse, molecularly imprinted polymers for creatinine by modified	

precipitation polymerization and their applications to creatinine assays for human serum and urine, 288-294, 2013, with permission from Elsevier.	22
Figure 3-5. SEM images of a creatinine (a) MIP and (b) NIP. Scale bar is five micrometers [6]. Reprinted from <i>Pharmaceutical and Biomedical Analysis</i> , Vol 85, Chitose Miura, Noriko Funaya, Hisami Matsunaga, Jun Haginaka, Monodisperse, molecularly imprinted polymers for creatinine by modified precipitation polymerization and their applications to creatinine assays for human serum and urine, 288-294, 2013, with permission from Elsevier.	24
Figure 3-6. Principle polymerization reaction of creatinine, DVB, and MAA [36]. Reprinted from <i>Medical Devices and Sensors</i> , Vol 3, Issue 6, Sumedha N. Prabhu, Subhas C. Mukhopadhyay, Chinthaka P. Gooneratne, Andrew S. Davidson, Guozhen Liu, Molecularly Imprinted Polymer-based detection of creatinine towards smart sensing, 2020, with permission from Wiley Online Library.	26
Figure 3-7. NIR absorbance spectra of creatinine [39]. Reprinted by Permission from RightsLink: Springer Nature, <i>Advanced Biomedical Engineering</i> , I. Suzuki, "Reagentless Estimation of Urea and Creatinine Concentrations Using Near-Infrared Spectroscopy for Spot Urine Test of Urea-to-Creatinine Ratio," <i>Advanced Biomedical Engineering</i> , vol. 7, pp. 72-81, 2018.	29
Figure 4-1. Schlenk line apparatus for freeze-pump-thaw degassing method [44].	33
Figure 4-2. MIP synthesis apparatus diagram. Atop a hotplate is a silicon oil bath in which a 3-neck flask was submerged in to control synthesis temperature. Stir bars are placed in both the oil and flask to promote homogeneity. The left neck of the flask (a) was only used to dispense reaction components and was sealed off during synthesis. The top neck housed a Liebig condenser, which was provided cool water (b,c) to help condense evaporated solvents. The right neck was used to perfuse the headspace with pure nitrogen gas (d,e) to prevent undesired reactions with oxygen molecules.	34
Figure 4-3. MIP synthesis apparatus photograph.	35
Figure 4-4. Lambda 950 spectrometer.	36
Figure 5-1. Freshly polymerized MIP (left: agitated in solution).	39
Figure 5-2. Sigma Aldrich vacuum filter assembly with vacuum pump.	41
Figure 5-3. MIP sample after drying.	42
Figure 5-4. View of UV WinLab software mid-capture.	43
Figure 5-5. Vials of creatinine solution containing MIP ("M0") and NIP ("N0"). Left photo taken after agitating the solution.	45
Figure 5-6. Absorbance versus concentration for the purified MIP samples.	47
Figure 6-1. All spectrometer spectra w/ averages for reference samples.	50
Figure 6-2. Absorbance and % transmittance for reference samples.	51
Figure 6-3. Area under curves for section of reference samples spectra.	51
Figure 6-4. Preliminary reference curve and respective residuals.	52

Figure 6-5. Reference curve boxplot.....	54
Figure 6-6. Impact of sample size on predictive accuracy.	55
Figure 6-7. Final reference curve.	55
Figure 7-1. Raman spectra for MIP, NIP, and creatinine samples.	58
Figure 7-2. SEM image of MIP sample.	60
Figure 7-3. SEM image of NIP sample.	61
Figure 7-4. Zoomed image of singular NIP microbead.	62
Figure 10-1. NIR spectra for creatinine solutions. Legend depicts concentrations in mg/dL.....	71
Figure 10-2. Derivative of NIR spectra for creatinine solutions. Legend depicts concentrations in mg/dL.	72

ACKNOWLEDGEMENT

I would like to express my sincere gratitude to Rensselaer Polytechnic Institute for allowing me the opportunity to pursue a challenging and rewarding academic career that has led to this exciting point. Special thank you to the Materials Science department for accepting me into this program and inciting me to express my passion through writing this thesis. Finally, I would not be here without my family, who have been unconditionally supportive in every step I have made in this ongoing journey.

ABSTRACT

The availability and timely use of novel diagnostic tools often benefits the prognosis and progression of many common diseases, including chronic and acute kidney disease, through better allotment of scarce treatment resources. Current renal diagnostic technologies employ organic (enzyme-based) sensing elements into devices that measure creatinine, a well-cited proxy for renal health found in serum and urine. While organic sensing elements are sensitive and specific, increased proliferation of the technology is restricted by cost, durability, and reusability concerns. This paper investigates the use of a polymer-based inorganic receptor material (molecularly imprinted polymer, or MIP) for sensing creatinine and demonstrates the viability of assessing MIP function using UV-VIS spectroscopy methods for detection of creatinine in solution. Results demonstrate that synthesis of microbeads of a creatinine MIP requires strict environmental controls, and that the detection of creatinine in pure solutions is possible in the UV-VIS range, but valid detection becomes more difficult once solutions have been exposed to the MIP due to polymer leachate entering the sample solution.

1 INTRODUCTION

The pressing need for elevating diagnostic technology standards has rightly revealed itself in the past few years. Even a routine blood test can now provide clinicians with thousands of critical quantitative data points on a person's health, where an early diagnose of disease, disorder, or infection can benefit the overall clinical outcome. Currently, this is all possible through organic molecule-specific diagnostic sensing elements.

Going beyond diagnosis, all-too-common ailments such as chronic kidney disease (CKD) require frequent monitoring of disease progression beyond clinical inception. CKD impacts the lives of 15% of the world's population and may manifest itself silently, but in many years result in total kidney failure where dialysis or a transplant are then required for survival [1].

Tools to monitor CKD and its related acute kidney injury (AKI) help clinicians to optimize individual treatment options for their patients, and to better allot scarce treatment resources such as transplant organs and dialysis machines. The increasing average age of populations and the occurrence of comorbid acute kidney injury in coronavirus-positive patients is what contributes to the greatest lack of resources in recent years [2] [3]. All the while, the number of transplantable kidneys has remained relatively constant, resulting in the most profound disparity between donors and awaiting recipients for any transplantable organ (Figure 1-1). Additionally, the unavailability of qualitative diagnostics surrounding kidney transplant processes has been demonstrated to result in the discard of thousands of otherwise transplantable organs [1].

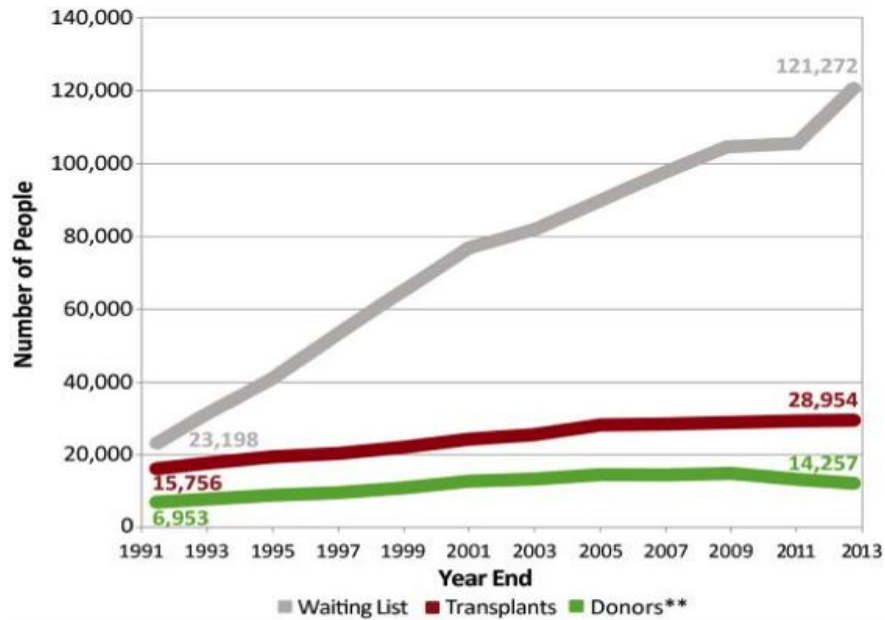


Figure 1-1. Kidney transplant statistics [4].

As it stands, the golden standard of molecular-based kidney disease diagnostics is expensive and not durable, and therefore practically unfit for the growing needs from those who suffer from the disease. This thesis explores a novel, inorganic type of sensing material, a molecularly imprinted polymer (MIP), which aims to provide a sensitive and selective alternative to sense a molecular kidney disease marker, but without the labor, expenses, and durability concerns of the current standard.

This work builds off of two recent publications by Miura et al out of Japan, who were able to synthesize an MIP which sufficiently sensed a kidney disease marker in both human serum and urine [5] [6]. Here, the aim is to replicate their synthesis work, and expand obliquely by assessing the synthesized material using spectroscopy to measure functionality—something assessed via chromatography in Miura et al.’s publication [6]. Compared to spectroscopy, the complexity of using chromatography is one dampener on the efficiency of researching this material. Note that molecular sensors containing MIPs are just starting

to bridge the gap from academia to commercialization, and hence these ideas are still in their inception phase and will be treated as such.

To explore this concept, first the necessary background (Section 2) and theory (Section 3) will be relayed, followed by four experiments which respectively aim to synthesize the MIP, visualize the MIP, provide a means to verify MIP functionality, and characterize the MIP as a standard ligand-receptor system. Ultimately, the synthesis of imprinted polymers yielded insightful SEM images and Raman spectra, however the use of spectroscopy for detection of creatinine proved difficult once solutions had become exposed to the polymers (versus detecting creatinine in pure aqueous solutions). Nevertheless, this research is one foundational step forward in characterizing this new material.

2 MOTIVATION

2.1 GLOBAL HEALTHCARE STANDARDS

In the past year, the publicization of medical diagnostic technology has reached new heights. Both the professional and general public's understanding of how viruses function, though at different depth levels, have been equally important in accelerating the field of medical diagnostics against the Covid-19 pandemic. One point of interest is how the greatest challenge was not necessarily technical, but logistical in terms of enabling availability and inciting the general public of the world to utilize these new medical tools. This phenomenon is well-rooted in first-world countries: academia and frontier biotech companies can and will continue to redefine the limits of what is possible, but there still exists large blockades in society that harshly limit the utilization of these novel technologies, as will be expanded on later in this paper. Optimistically however, these recent breakthroughs in medical diagnostics have spanned beyond Covid-19, which brings optimism that in future years commercialization in this field will continue to expand its reaches across the globe.

This optimism is held because while scientists and engineers have come a long way, there are still many victims of diseases whose poor diagnoses lead to less favorable outcomes than is possible, especially being the case in resource-limited environments. In support, malaria, the most common parasitic disease in the world, still heavily relies on lab-based microscopic analysis to determine the presence of the disease. This disease is more prolific in African countries due to its preference for higher temperatures; however, this is also where lower GDPs ultimately diminish the availability of novel laboratory diagnostic testing. Even with these tests, optical methods cannot distinguish the type of malarial disease, and cannot catch it at its onset—where treatment options are more effective [7]. Furthermore, there are numerous other ailments including kidney diseases—the focus of this paper—that benefit greatly from continued

diagnostic testing throughout the disease progression—this is another challenge with traditional lab technology. Hence, both the validity and availability of diagnostic tools are equal key specifications for improving global healthcare outcomes.

2.1.1 Kidney Disease

As mentioned, diagnosing and monitoring kidney disease is the primary motivator for this research. Kidney disease, or renal disease, is a detrimental group of conditions no matter one's place in the world. About 15% of the general population lives with chronic kidney disease, or CKD, a disease characterized by a progressive loss in renal function over the course of years to decades. Symptoms range from fatigue, to edema, to hematuria (blood in the urine), and if left untreated is deadly for those 500,000 people in the U.S. with kidney failure, who require frequent dialysis or a viable kidney transplant to survive [1].

To better understand these symptoms, the kidney's four main functions as a blood filter are briefed: fluid (blood, interstitial, lymphatic) volume balance, electrolytes (sodium, potassium) balance, blood pH balance, and waste excretion—with urination ultimately being that process that permits these bodily changes. About two-million functional units called nephrons can be found in each human kidney (see Figure 2-1, explained further shortly), each of which takes in blood and filters it to choose what it wants to keep. CKD permanently limits some nephron's ability to perform these vital functions, often due to chronic inflammation and sclerosis, which ultimately throws off the delicate balance in our bodies (our "homeostasis"), resulting in the need for clinical intervention. At this time, there is not cure for chronic kidney disease, only lifestyle changes that may slow its progression.

The other half of kidney disease is acute kidney injury (AKI), which is present in roughly 50% of all ICU patients to some degree, as a side effect of another ailment [1] [8]. The manifestations are similar to CKD

but only exhibit themselves for a few days and is deadly only under certain comorbid conditions—such as being infected with the Covid-19 virus [3].

Therefore, monitoring CKD and AKI is important both for addressing the onset of the condition but also the progression of these ailments that can take from days to decades to fully progress. This difference in timing means allotting proper medical treatment, such as dialysis machines or getting on the transplant waiting list (where the average wait time is 4.5 years), is more efficient and logistically sound when quantitative patient data is available to clinicians [1]. Patients on the wait list most likely require frequent dialysis treatments, and as a result suffer a significant detriment to their quality of life.

2.1.2 Quantifying Kidney Function: Creatinine

From the prior statements, it is unsurprising that the concept of quantitatively monitoring renal function has become a well-cited topic. The most common test of renal function is a creatinine clearance test. Creatinine is a small biological molecule (113 Daltons) which is a degradation product of creatine and creatine phosphate, which facilitate ATP production. The kidneys act to excrete creatinine by freely allowing it through its filtration mechanisms, ultimately excreting it through urine. This “free filtration” aspect combined with a fairly stable serum concentration means that the amount of serum being filtered by the kidneys, known clinically as glomerular filtration rate (GFR), can be estimated mathematically using the mass amount of creatinine one’s body excretes (or “clears”) over a certain amount of time—typically 24 hours (Figure 2-1). GFR, which is a flow rate which fluctuates between 80 and 120 mL/min for a healthy adult, is the primary metric tracked for progression of chronic kidney disease, and for the recovery of acute kidney injuries [9].

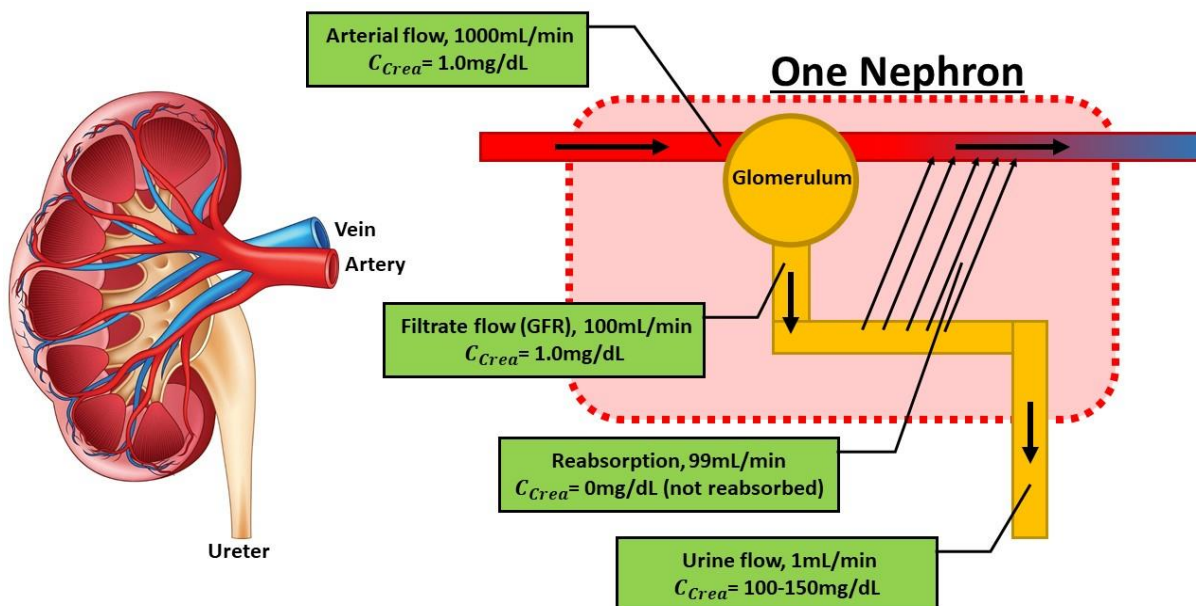


Figure 2-1. (left) Basic anatomy of a human kidney [10]. (right) Flow geometries of the kidney demonstrated as the flow within one nephron. " C_{Crea} " is the concentration of creatinine in the respective vessel, demonstrating how creatinine is freely filtered by glomeruli and not effected by the reabsorption mechanisms present for moving fluid/solutes from the tubules (yellow) back into the renal vasculature (red/blue).

Stepping back, creatinine itself is not a structurally-unique molecule in serum, which historically has made its reliable quantification in solution a difficult feat. Miura et al provides a useful graphic of structurally-similar compounds to creatinine, like creatine (6) and pyrrolidone (4) (Figure 2-2). Urea, another biomarker used for kidney function, is less similar than those in Figure 2-2 but present in larger quantities in serum. Even just the presence of a similar carbonyl group can make these low molecular weight species difficult to distinguish using methods such as spectroscopy, as is briefed in the following section 3.3. Despite these challenges, an early version of creatinine testing arose at a time when scientific medical diagnostics was still in its infancy.

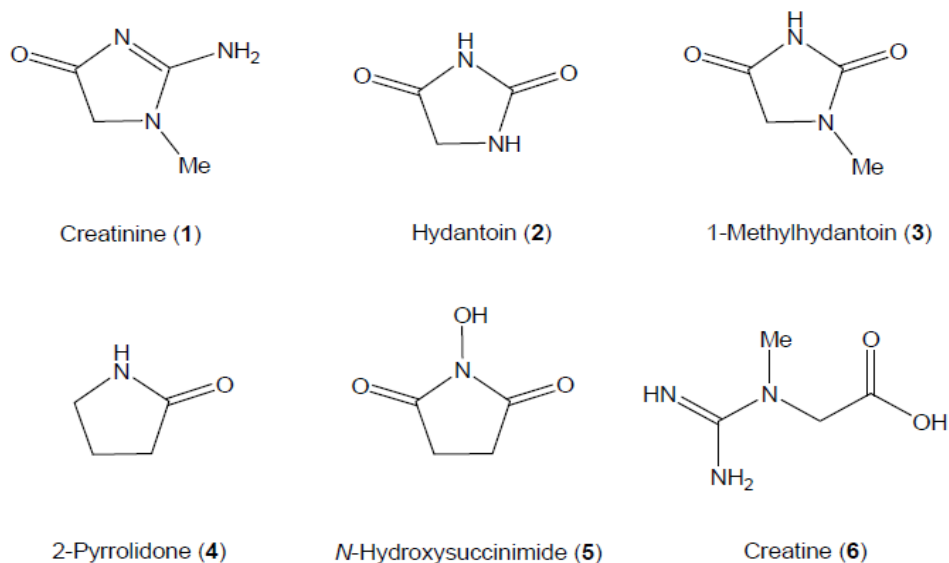


Figure 2-2. Creatinine and five molecularly-similar compounds found in bodily fluid [6]. Reprinted from *Pharmaceutical and Biomedical Analysis*, Vol 85, Chitose Miura, Noriko Funaya, Hisami Matsunaga, Jun Haginaka, Monodisperse, molecularly imprinted polymers for creatinine by modified precipitation polymerization and their applications to creatinine assays for human serum and urine, 288-294, 2013, with permission from Elsevier.

2.1.3 Diagnostic History: The Jaffe Method

In 1886, Max Jaffe published a paper in Germany detailing the reaction of picric acid with creatinine (Figure 2-3) alongside other organic molecules like glucose, ascorbic acid, ketones, and forms of heparin [11] [12]. Reaction with these analytes results in similar modifications to the picric acid which is detectable colorimetrically using a spectrometer. Despite being largely inaccurate, the ability to discern chronic kidney disease at all was its own achievement in those early years, because as mentioned this is a disease that eventually requires treatment. However due to the non-selectivity of the test, the Jaffe method is now obsolete, and for the purposes of this argument will not be considered a molecular-sensing form of diagnostics. To Jaffe's benefit, the fundamental principles he utilized for this test were not forgotten after his time, as is described next.

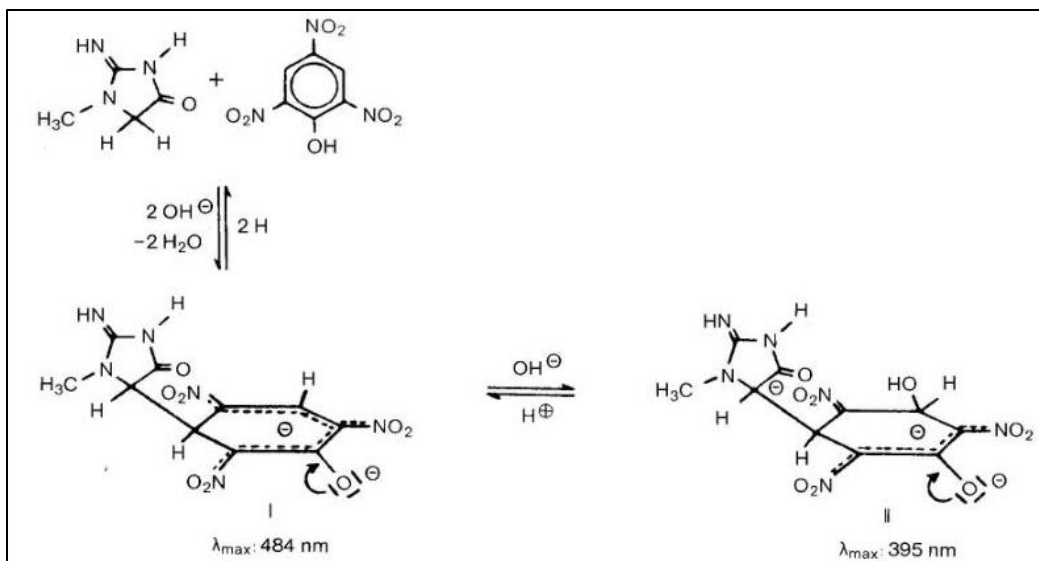


Figure 2-3. Jaffe method principle reactions. Top displays reactants: creatinine and picric acid. Bottom displays the two forms of the complex resulting from the spontaneous reaction of the reactants, and their respective detectable wavelengths [13].

2.2 MOLECULAR SENSING

As a response to the need for improved globally available diagnostic tools, recent decades of literature have been obsessed with the novelty of the “biosensor”, and rightfully so. Biosensors are elegant diagnostic systems that directly detect the thousands of unique compounds present in the cells and fluids of our body, ultimately yielding better medical precision and patient-personalized solutions. According to a brief article by InsightsCare, the molecular diagnostics industry is valued at \$7.5 billion dollars as of 2017, and is predicted to rise to \$24.6 billion by 2024 [14]. Their recent success is largely attributable to increased sensitivity, selectivity, and fast detection on devices which aim to lower cost and user requirements. Understanding their basic functionality will help cement these benefits, but also shine some light on the drawbacks of current practices [15].

2.2.1 Today's Golden Standard

One aspect of biosensors is their ability to sense, transduce, and relay an interpretable signal back to the user. These three steps are also engrained in most general sensors; for example, a thermistor senses local changes in temperature by having an internal piece of metal wire heated up, through which a known voltage is applied. The resulting resistance through the metal is temperature-dependent—this electrical current is the transduction method, which can be interpreted with some simple external circuitry.

Moving forward, the transition into molecular sensing systems has primarily relied on biomimicry, which is the concept of replicating organic systems for our own purposes. The biomimicry in question is the antibody-antigen system—the basic lock-and-key, respectively, that our bodies use to selectively recognize and bind desired molecules (Figure 2-4, left) [15].

An antigen is any molecule that the organism has an antibody for. Antibodies are protein structures, ranging from a couple hundred to tens of thousands of Daltons in weight [15]. These protein structures are long chain(s) of amino acids, which have a specific folding structure that elicits a unique binding site for the specified antigen (Figure 2-4, right).

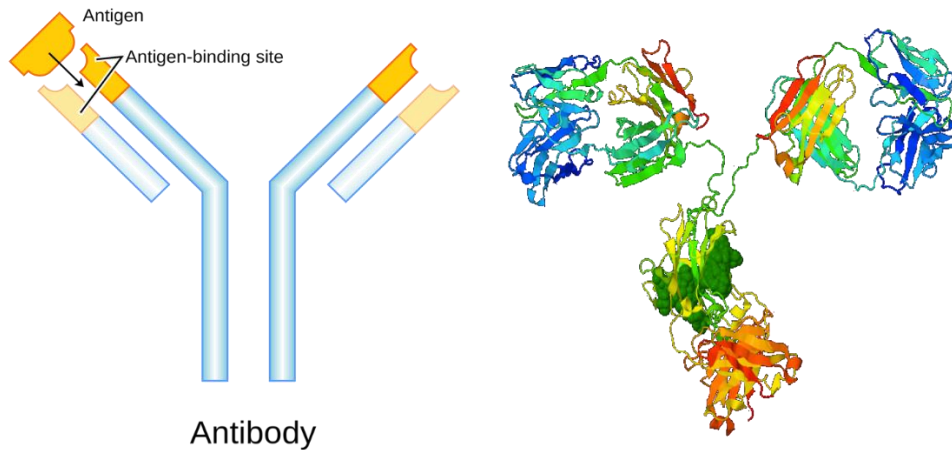


Figure 2-4. (left) Example of an antibody containing an antigen binding site for the reciprocal antigen (in yellow). (right) Simulated protein structure of an antibody, demonstrating how the folding of different protein chains to form one larger unit [16].

One commercially successful manifestation of the antigen-antibody system is in the form of an enzyme-linked immunosorbent assay, or ELISA. Briefly reviewing a creatinine ELISA will help in highlighting the strengths and weaknesses of this golden standard.

2.2.1.1 Creatinine ELISA

The ELISA highlighted here is Lifespan Bioscience’s (LSBio) “Bovine Creatinine ELISA Kit (Competitive EIA)”, which was chosen due to its resemblance to the standard of ELISAs [17]. This assay is used to quantitatively detect the presence of creatinine in plasma, serum, and tissue homogenate—with the latter being used to evaluate the metabolic capability of certain tissues, which is an additional clinical use of creatinine sensing that has not been mentioned up to this point.

The principle function of the ELISA is demonstrated well in the following image supplied by LSBio’s user manual (Figure 2-5). In summary, LSBio supplies microtiter plates that have been pre-coated with the antigen, creatinine. Into each well sample solutions are added, after which the supplied antibody for the antigen is added in a known quantity. Next the antigens “compete” for antibodies, with the ratio of

adhered to free antigen-antibody complexes then depending on the concentration of creatinine in the sample solution added. From here, the solution is washed away, and horseradish peroxidase (HRP), an enzyme, is added in solution to the wells. HRP binds to a portion of the antibody, which activates it, with the extra being washed away. Finally, 3,3',5,5'-Tetramethylbenzidine (TMB) is added in solution, which reacts with the activated HRP enzyme to elicit a product detectable colorimetrically at a 450nm wavelength [17]. A plate reader or similar spectrophotometer is required to deduce an absorbance value, which is then related to the sample solution creatinine concentration via standardized calibration data.

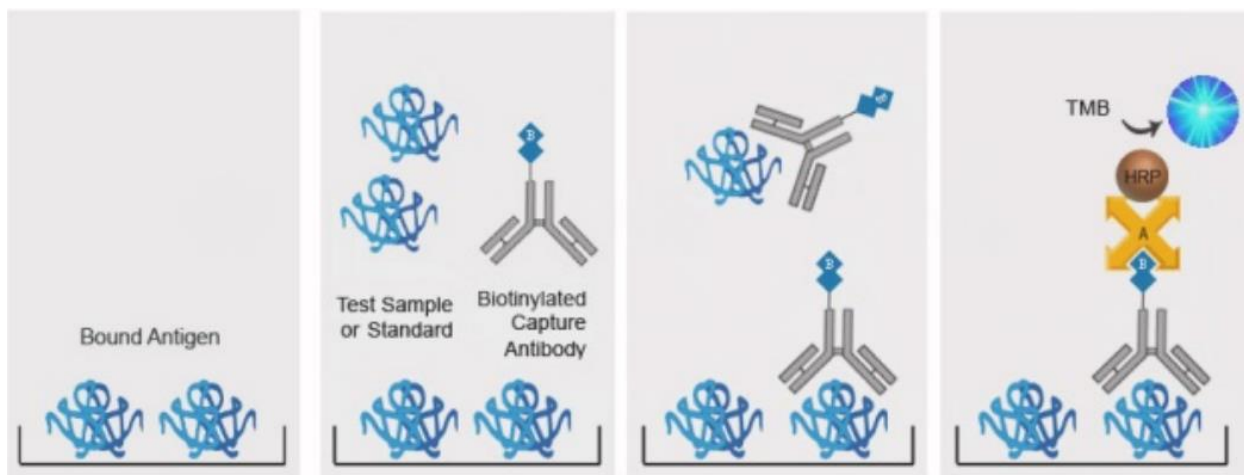


Figure 2-5. Principle function diagram provided by LSBio for their creatinine ELISA kit, see above text for details [17].

Functionally, the use case of the assay is well-bounded, in that while serum creatinine values are within its range, most urine creatinine values (which possess clinically-relevant data) would be beyond this range (0.781-50 ug/mL). Each kit, containing one 96-well plate (which is a one-time use plate), is priced at \$740, which for lab work is often feasible, but clinically is **not** when considering that daily assays can be needed—and with rapid results [17]. Both the price and single-use limitations are a result of the use of these multiple biological components, especially the creatinine antibody. Beyond the R&D, this antibody

requires complex bioreactors to fabricate—the option for in-house protein synthesis is not at all a common feature in most labs. Even once customers have this device in-hand, they must be kept at 4°C, which further deters from how practical these assays are in low-resource settings.

Nevertheless this ELISA kit and many others do serve important purposes in R&D applications; the following (Table 2-1) is used to summarize the aspects of enzymatic-based assays/sensors to highlight their strengths and what may be preventing further proliferation of the technologies; and this will be referenced to later in this paper, after a new type of biosensor is introduced. Helpful here is that the terms assay and sensor may be used interchangeably due to the dependence on the application, but formally one could coin an assay a one-time detection method, whereas sensors may provide more than one use—often with recalibration involved.

Note there are other types of enzyme-based assays that share qualities equal to those mentioned, such as ones that utilize enzymes to catalyze reactions directly to the antigen, resulting in a product that is then detectable. A creatinine assay of this nature exists which utilizes a multi-step reaction to produce hydrogen peroxide, which is detectable via electrochemistry [18].

Table 2-1. Typical pros and cons of enzyme-based molecular sensors.

Quality	Pro	Con
Sensitivity:	High sensitivity	Often range is sacrificed.
Selectivity:	Highly selective	
Fabrication:	--	Requires complex machinery.
Use case:	Some sensors can be re-used.	Often single use assays.
Cost:		High due to biologics.
Storage:	Stable when frozen.	Requires constant freezing temperatures.
Usability:	--	Requires a plate reader and frequent calibration. Skill worker preferred.

2.2.2 Creatinine's Future

In the prior section the premise of another type of creatinine sensor was acknowledged—one utilizing a chemical reaction on creatinine itself to produce a detectable signal via enzyme catalysis. In general, there are a few varieties of creatinine sensors available, but this section is meant to reiterate that the need statement is not necessarily how to *best* sense creatinine in biological fluid, but instead it is how to best sense the ability of the kidney to clear fluid and excrete it via urination.

Hence, creatinine is not the only solution to this growing issue of renal disease and diagnostic care. Similar molecules which share the kinetics of creatinine may be used to determine renal filtration (see section 2.1.2 for the review on renal physiology). Exogenous, or not naturally-occurring, compounds such as iohexol and inulin (Figure 2-6) may be infused into a patient's blood, and the rate at which the kidney filters them can be estimated using the mass excretion through urine (Equation 1).

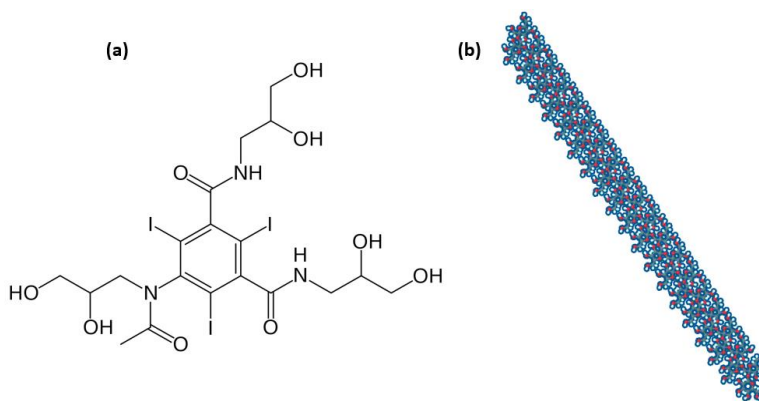


Figure 2-6. (a) Structure of iohexol, and (b) structure of inulin. Inulin containing repeating carbohydrate units [19] [20].

$$MassFlow \left(\frac{mg}{min} \right) = FlowRate \left(\frac{mL}{min} \right) * Concentration \left(\frac{mg}{mL} \right) \quad (1)$$

Due to the drawbacks in Table 2-1, researchers in this decade have been rethinking the need for organic compounds in biosensors, and recently have begun to discover some of the most elegant solutions yet.

3 THEORY

3.1 SYNTHETIC RECEPTORS – MIPs

In recent years, the academic proliferation of a new type of sensor, the molecular imprinted polymer (MIP), has come to light (Figure 3-1). A paper by Miura et al has introduced this sensor material variant to creatinine sensing—the aims of this thesis are to expand on and provide more detail into the characteristics of the concept this group explored. But first, the key qualities of this novel idea will be introduced.

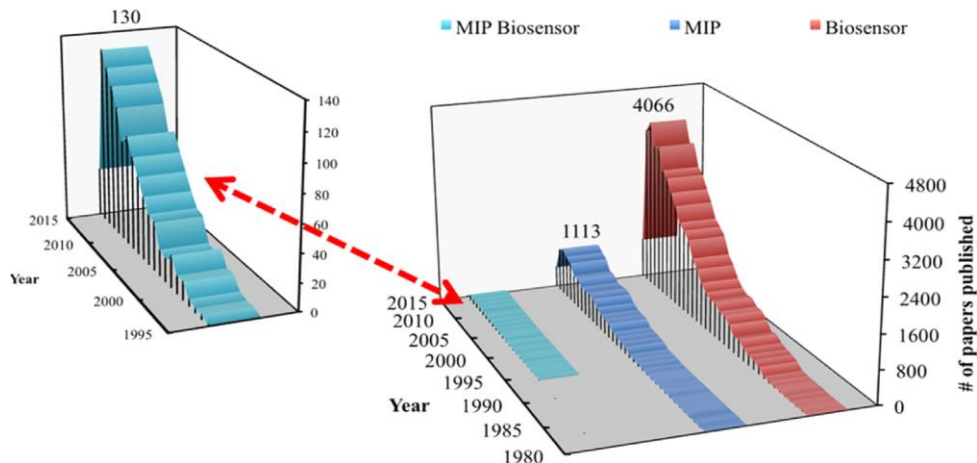


Figure 3-1. Number of publications with respect to time for MIP biosensors, MIPs, and biosensors, respectively [21]. Reprinted (adapted) from J. Belbruno, "Molecularly Imprinted Polymers," *Chemical Reviews*, vol. 199, no. 1, pp. 94-119, 2018.. Copyright

2021 American Chemical Society.

The inception of the molecularly imprinted polymer predates the enzymatic biosensors described above. Yet, there was an understanding of the organic antigen-antibody relationship, and this was the base for a variety of experiments aimed at creating an analog to this organic lock-and-key system. At its inception is

the work of George Wulff and A. Sarhan, who were looking to sense specific compounds in racemic mixtures [22]. Their early concepts to replicate synthetic, specific receptors (the “antibodies”) were quite elegant: their premise is that a polymer would be synthesized from solution, where the antigen would also be present. Polymerization results in the entrapment of antigen within the resulting material, which if extracted left a perfect antigen-shaped “hole” in its place; in theory this is where another antigen could bind, resulting in one of the earliest forms of a synthetic molecular receptor [23].

Since the 70’s, molecularly imprinted polymers have come a long way, but their intent is still the same: to provide a simple, variable method for creating molecular receptors without the use of organic substrates. The rest of this section 3.1 details the mode of function, key specifications, how to functionally characterize, and how to synthesize MIPs.

3.1.1 MIPs: How Do They Work?

To understand the workings of an MIP material, the typical fabrication and use case is briefed. To fabricate an MIP, there are four main components required: a solvent, the functional monomer(s), a crosslinker, and the antigen (follow Figure 3-2 for illustrations). The solvent provides an environment for the other components to react in. In this paper and in most cases, porogenic solvent(s) like acetonitrile are used to promote porosity in the final polymer product [5]. The functional monomer can be described as the intermediate between the matrix polymer and the antigen—it is meant to become part of the polymer matrix, but also possesses side groups that will form weak bonds with parts of the antigen compound, which is a kinetic process that begins in solution (i.e. the “pre-complex” shown in Figure 3-2). Finally, upon polymerization the crosslinker promotes covalent bonding between pre-complexes, which ultimately yields the final material.

Section 3.1.4 further describes synthesis methods, but typically these components will be dissolved in solution, where polymerization induced by heat and/or initiators can begin. Resulting from this is a bulk or powdered polymer, in which the antigen is trapped, being bound loosely to neighboring functional “monomers” (which have been polymerized) [21] [24].

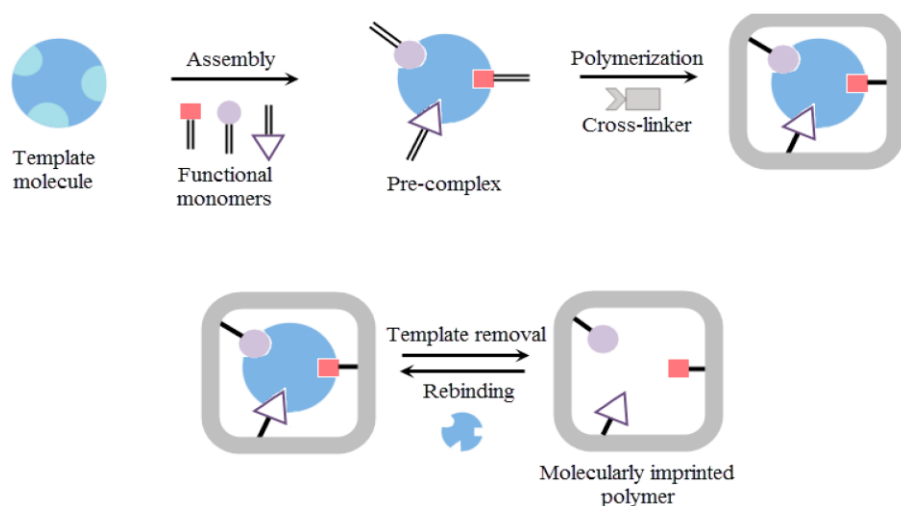


Figure 3-2. Principle steps for MIP synthesis and function. See text for details [21]. Reprinted (adapted) from J. Belbruno, "Molecularly Imprinted Polymers," *Chemical Reviews*, vol. 199, no. 1, pp. 94-119, 2018.. Copyright 2021 American Chemical Society.

The second part of Figure 3-2 demonstrates the elegance of the polymer created: due to the weak bonding between antigen and functional monomer(s), extraction of the antigen is achievable often with a basic solution of ethanol, for example. Doing so leaves these antigen binding sites empty, which will only be repopulated when that specific antigen comes into suitable contact with the MIP. The process of antigen extraction and rebinding is repeatable, which takes us into the next section which specifies the aspects of the material resulting from this unique but simple synthesis method. Antigen presence in the polymer is

detectable using wide array of methods including spectroscopy and impedance, but this is beyond the scope of this paper [21].

3.1.2 MIPS – Key Specifications

Earlier in section 2.2.1.1 the typical qualities of an enzyme-based biosensor were demonstrated via Table 2-1. The subsections here will compare that information to the qualities proposed by MIP biosensor theorists, with most information for the MIPs coming from a review in 2017 by Belbruno et al [21]. Specific quantities to compare are pulled from the creatinine ELISA covered earlier, and the work of Miura et al for their creatinine MIP concept [17] [5] [6].

3.1.2.1 Sensitivity

Molecular sensing of creatinine is unique in that it is clinically relevant both in blood serum and urine, where concentrations for the latter may be up to two orders of magnitudes higher as a result of the fluid reabsorption aspect of kidney function [10]. This is a wide detection range for any device; including LSBio's creatinine ELISA, which has a detection range of 0.781 to 50 µg/mL [17].

Comparing this to Miura et al's creatinine MIP concept, we see this group has used the same material to accurately evaluate creatinine concentrations ranging between 0.5 to 2,000 µg/mL [6]. Granted while there stands no verification testing on this concept, the three-orders of magnitude range still holds lots of promise for a potential diagnostic device that can be used with both serum and urine samples.

3.1.2.2 Selectivity

If antibody-antigen systems were *not* selective, our bodies would have a difficult time functioning. Thankfully MIPs share this trait due to the nature of their synthesis, and the following section 3.1.3 will expand on this. Where MIPs excel compared to antibodies is the restrictions on the type of antigens

detectable. Figure 3-3 demonstrates the wide range of imprintable templates possible with MIPs; antibodies, especially for the larger molecules, are more difficult or are currently impossible to fabricate [23].

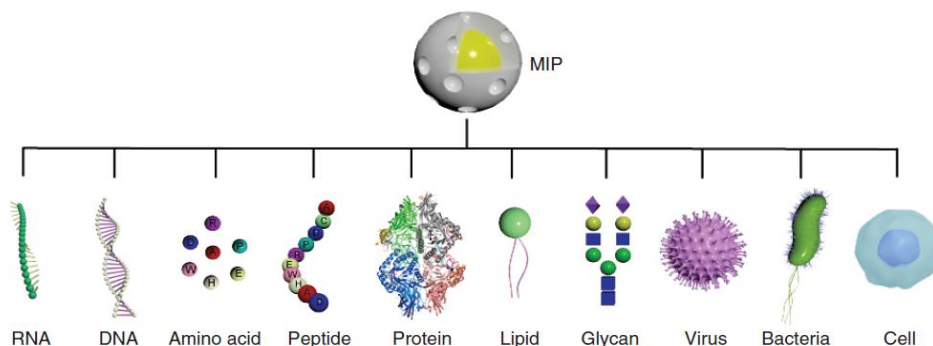


Figure 3-3. Examples of the numerous, imprintable templates for MIPs [23]. Reprinted from BioTechniques, Vol 69, Zahra El-Schich, Yuecheng Zhang, Marek Feith, Sarah Beyer, Louise Sternbæk, Lars Ohlsson, Maria Stollenwerk and Anette Gjørloff Wingren Molecularly imprinted polymers in biological applications, 407–419, 2020, with permission from Creative Commons.

3.1.2.3 Stability/Storage

The polymeric nature of an MIP means its shelf life is inherently longer than that of an enzymatic sensor (at temperature greater than -80 degrees centigrade) [21]. The inert nature of the material elicits minimal reactions with the environment, promoting durability at normal operating temperatures.

3.1.2.4 Biocompatibility

Stemming off from improved stability, the inert nature of most polymers means that biocompatibility is not a large concern. Molecular biosensors most often are exposed to bodily fluids like serum or urine; and if this fluid is not ex situ to the body when sensing is done, then the interaction of the material with the body must be characterized. This comes in terms of acute/chronic reactivity, immunological responses, and the possibility for degradation products entering the body [21]. FDA and ISO documentation such as ISO-13485 and ISO-10993 provide the details necessary for identifying and evaluating these concerns.

3.1.2.5 Fabrication (cost/labor)

Polymers are inherently batch-friendly, and with the bulk consisting of [functional] monomers such as methyl methacrylate (MAA), acrylic acid (AA) or acrylamide (AAM), material cost is minimal [25]. Porogenic solvents such as acetonitrile or toluene are also inexpensive; the antigen (template) is the main variable here. Synthesize apparatuses for both MIPs and enzymatic may be comparable on a larger manufacturing scale—however the average complexity of research and development for novel antibody-based sensor materials supersedes that of an MIP.

3.1.2.6 Integration complexity

Integration complexity is another way of describing how disruptive the integration of these technology into pre-existing systems would be. This includes skilled labor requirements, alterations from standard protocols, different time/tool requirements, and the overall willingness of the users to accept a new technology into their systems.

While these qualities are not the focus of this paper, they are kept in mind because logistics can make-or-break any new technology, no matter how revolutionary.

3.1.3 MIP Functional Properties

Verification of an MIP material as a sensing element (receptor) is demonstrated through three intrinsic functional properties: imprinting factor (I.F.), binding capacity (B.C.), and response time (R.T.). To deduce the properties, often a *non-imprinted polymer* (NIP) variant must also be fabricated; this is a control that should be synthesized exactly as the MIP, barring the inclusion of the antigen in the synthesis solution.

Imprinting factor (I.F.) is how selectivity (see section 3.1.2.2) is quantified. Technically, I.F. refers to the preferentiality of how much antigen binds to the MIP in reference to the NIP. Typical values here range in the single digits [21]. This value must sufficiently supersede imprinting factors of known interfering agents;

for creatinine, Figure 2-2 displays a couple of those structurally similar compounds. Miura et al has already deduced imprinting factors for this creatinine MIP (Figure 3-4); their process involved HPLC, and recording different elution times, to yield retention factors (Equation 2), and ultimately the imprinting factors (Equation 3) for each analyte on the MIP [6].

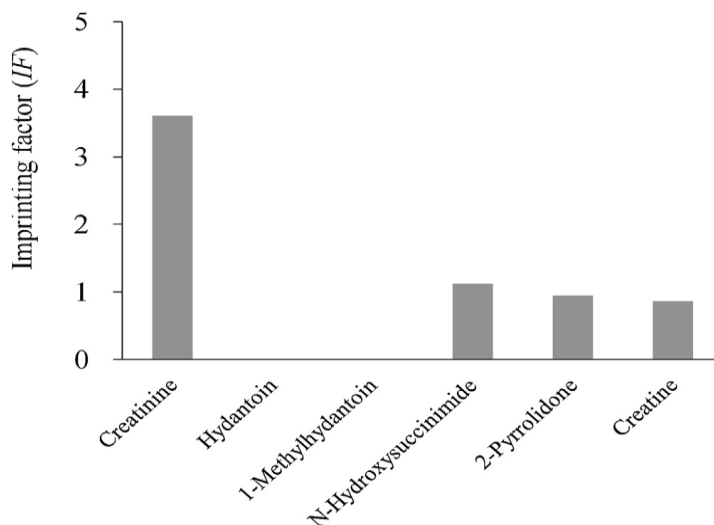


Figure 3-4. Imprinting factors for creatinine MIP against five structurally-similar compounds [6]. Reprinted from *Pharmaceutical and Biomedical Analysis*, Vol 85, Chitose Miura, Noriko Funaya, Hisami Matsunaga, Jun Haginaka, Monodisperse, molecularly imprinted polymers for creatinine by modified precipitation polymerization and their applications to creatinine assays for human serum and urine, 288-294, 2013, with permission from Elsevier.

$$\text{retention factor, } k = (t_R - t_0)/t_0 \quad (2)$$

$$\text{imprinting factor, } IF = k_{MIP}/k_{NIP} \quad (3)$$

Binding capacity (B.C.) is the standardized variable for determining the sensitive range of an MIP. Quantitatively, Boysen et al details B.C. as “the ratio of the concentration of the target molecule absorbed from solution divided by the initial concentration of initial solution” [25]. B.C. is better understood through

parameters Q_{\max} and k_d , which respectively are the standardized max number of binding sites and the disassociation constant of the MIP [26]. These are deduced via a Scatchard analysis, which is detailed independently in section 3.4 as it an essential part of MIP characterization.

Response time (R.T.) does not have a concrete description across all applications, but one definition deems it the “the time required to reach 63.2% of the final signal from when the stimulus was applied/exposed” [25]. R.T. will not be a focus in this thesis, but it should be understood that different synthesis techniques can drastically alter the diffusion kinetics related to antigen binding/extraction which are more relevant in a commercial device than in this academic proof-of-concept.

3.1.4 Precipitation Polymerization of MIPs

Method of synthesis largely effects the aforementioned MIP characteristics, especially with regards to the kinetic factors involved due to differences in the resulting surface areas and template density. Barring some frontier nano-patterning MIP research, most synthesis methods are centered on bulk polymerization from solution, or more specifically free radical polymerization [27]. The principle of this polymerization type is that it is heterogeneous: a continuous (solvent) monomer-rich phase houses a polymer-rich phase, with their existing a unique interface between the two phases [28].

This general method is referred to as dispersion polymerization if a surfactant is used to control polymer aggregate size (relates to polymer molecular weight distribution, MWD), and precipitation polymerization if one is not included. Regardless, the result is typically a fine powder of polymer microbeads. Miura et al utilized a standard precipitation polymerization with the aid of porogenic solvents to yield polymer microbeads with a high surface area (Figure 3-5) [5]. In theory this quality would quicken the response time, thus making processes such as creatinine extraction less tedious.

This thesis focuses on characterizing the equilibrium qualities of creatinine with the MIP, which is only somewhat dependent on the synthesis method. While optimizations to the synthesis process likely exist, this thesis will focus on characterizing the work of imprinted polymers already created due to the availability of existing data.

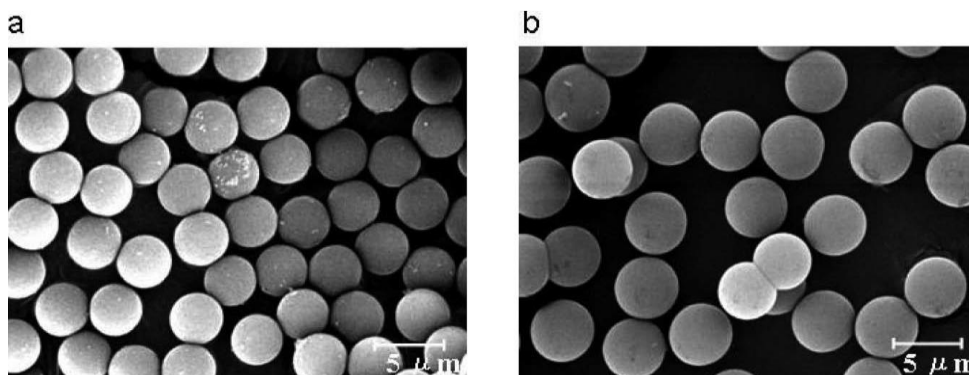

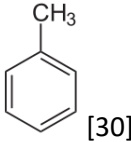
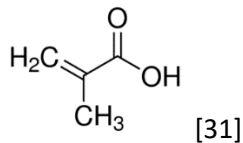
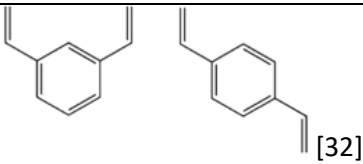
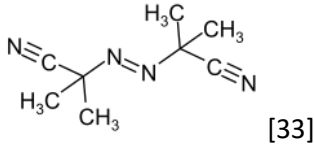
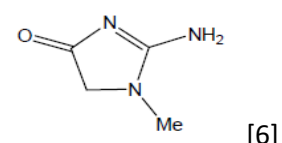


Figure 3-5. SEM images of a creatinine (a) MIP and (b) NIP. Scale bar is five micrometers [6]. Reprinted from *Pharmaceutical and Biomedical Analysis*, Vol 85, Chitose Miura, Noriko Funaya, Hisami Matsunaga, Jun Haginaka, Monodisperse, molecularly imprinted polymers for creatinine by modified precipitation polymerization and their applications to creatinine assays for human serum and urine, 288-294, 2013, with permission from Elsevier.

3.2 MIURA ET AL.'S CREATININE MIP

This section reviews the theory behind Miura et al.'s creatinine MIP, including the compounds used and how they are hypothesized to interact with one another and their environment during precipitation polymerization. The following Table 3-1 summarizes each compound used; review section 3.1.1 for more information on the “category” column.

Table 3-1. Each compound in the creatinine MIP detailed by Miura et al.

Name	Category	Molecular structure
Acetonitrile	Porogenic solvent	 [29]
Toluene	Porogenic solvent	 [30]
Methacrylic acid (MAA)	Functional monomer	 [31]
Divinylbenzene (DVB)	Crosslinker	 [32]
2,2'-azobis(isobutyronitrile) (AIBN)	Initiator	 [33]
Creatinine	Template	 [6]

Beginning with the heart of the MIP there is creatinine and MAA (Table 5-1). Recall that creatinine is the breakdown product of creatine, and its 113.12 g/mol weight consists of an imidazole ring with attaching methyl, amine, and ketone groups. The principle of the MIP is that methyl methacrylate (MAA) monomers will form “pre-complexes” in solution with creatinine; this is hypothesized to occur between hydrogens on one creatinine, and oxygen molecules on multiple MAA monomers [34]. Note that gaseous oxygen is expected to disrupt the homogeneity of these complexes; hence the following procedures will include a degassing process.

With these complexes formed, the next compound in action is the crosslinker divinylbenzene (DVB) (Table 5-1). Crosslinking is required to “cement” the pre-complexes in their current shape. DBV is a non-unique

choice; it is a simple, symmetric molecule that has two sites for polymerization, which when present in conjunction with the MAA polymerization sites will form covalent bonds under correct synthesis conditions. Weight fraction of the crosslinkers does impact MIP performance; higher weight fraction promotes a more rigid structure with increased yield capacity, which is more important when a porogenic agent is used to promote high porosity (i.e., lowering bulk density) in the final product, though at the cost of creatinine site density [35].

The theorized principle reactions between creatinine, DVB, and MAA are illustrated clearly by Prabhu et al below, who in late 2020 also expanded on the earlier work of Miura et al by implementing an electrochemical impedance spectroscopy (EIS) technique into characterizing the MIP [36].

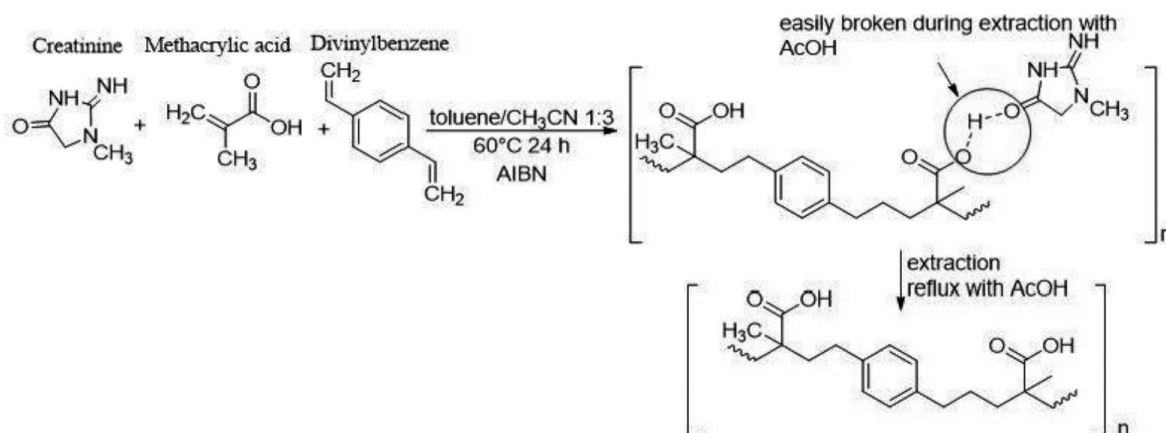


Figure 3-6. Principle polymerization reaction of creatinine, DVB, and MAA [36]. Reprinted from *Medical Devices and Sensors*, Vol 3, Issue 6, Sumedha N. Prabhu, Subhas C. Mukhopadhyay, Chinthaka P. Gooneratne, Andrew S. Davidson, Guozhen Liu, *Molecularly Imprinted Polymer-based detection of creatinine towards smart sensing*, 2020, with permission from Wiley Online Library.

Stemming from the prior paragraph, two porogenic solvents are used in this creatinine MIP: acetonitrile and toluene (Table 5-1). The solubility of creatinine, MAA, and DVB (the reagents) in these two solvents

is what impacts resulting polymer porosity, with poor solubility ultimately inducing the larger pore size achieved by Miura et al. A larger pore size benefits the response time of MIPs as noted in section 3.1.3. Briefly, porogenic solvents work because poor solubility (via Hildebrand values) means that polymer nuclei are better solvents to the reagents than the solvents themselves, thus [nuclei] aggregation is the preferred method of polymerization for the majority of the synthesis process [37].

The final ingredient is the initiator 2,2'-azobis(isobutyronitrile) (AIBN) (Table 5-1). AIBN catalyzes the reaction of MAA and DVB by lowering the activation energy required for the bonding to occur, hence drastically speeding up the nominal polymerization process. AIBN is not expected to be consumed during synthesis, hence its exact dosing is less significant to this process.

Overall, Miura's group utilized these reagents in a synthesis apparatus similar to the one described below in section 4.2, with their synthesis procedure also being replicated in section 5.1, albeit some minor discrepancies that are noted in their respective sections.

3.3 SENSING CREATININE IN SOLUTION

With every new sensing material there needs to be a method to verify its function; for this material it is that it binds with creatinine with a higher propensity than other molecules. The latter half of that statement was verified in a previous work by the Miura group, who determined imprinting factor as noted in the previous section [6]. In general, all of Miura et al's experiments on the MIP/NIPs utilized chromatography (HPLC) to determine the presence of solutes passing by the material. While this is a well-documented process for porous materials such as this, the knowledge, resources, and time required to replicate that process was not available. Hence, another means of detecting the binding of creatinine in

the MIP/NIP is hypothesized—one that improve the characterization efficiency in future works if deemed viable.

The essence of this different approach is that since it is much harder to detect the hydrogen bonding of creatinine to the polymer, the removal of creatinine from the solution which was exposed to the polymer is what will be measured. Here, this is done using optical techniques across different UV-VIS-NIR wavelengths; note that the concept of *just* using optics to determine the concentration of creatinine in solutions is its own field of research, with the main challenge there being the presence of many interfering analytes such as urea, glucose, proteins, ketones, and other nitrates in blood and urine [38].

Briefly in the NIR realm, there are two similar works, one by Suzuki et al in 2019 who built off earlier studies by Pezzaniti et al in the early 2000's. Focus here was first given to the Suzuki paper where the objective was to detect the presence of creatinine [and urea] in real human serum and urine solutions using standard LEDs ranging from 1400-2500 nm in 100-nm increments. In this NIR range they would be detecting the scattering resulting from the resonance of the LED waves with the different functional groups on those molecules. The result of this resonance is a change in the absorbance spectra as a function of the concentration of the solute (Figure 3-7).

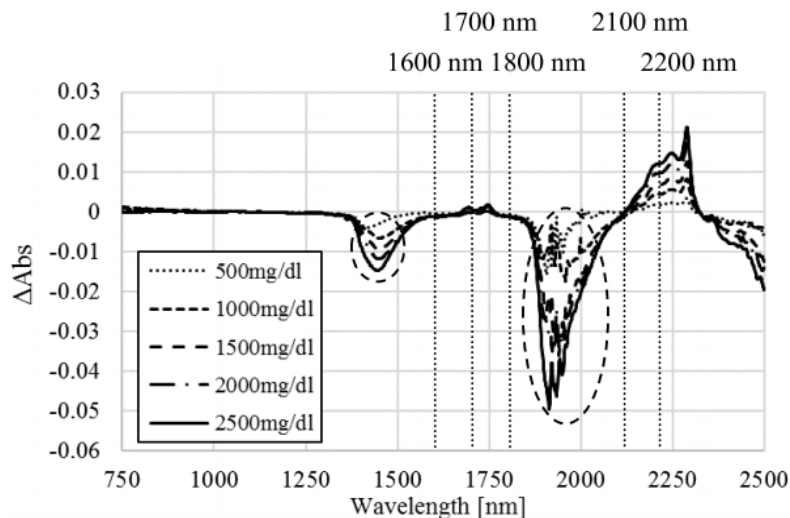


Figure 3-7. NIR absorbance spectra of creatinine [39]. Reprinted by Permission from RightsLink: Springer Nature, *Advanced Biomedical Engineering*, I. Suzuki, "Reagentless Estimation of Urea and Creatinine Concentrations Using Near-Infrared Spectroscopy for Spot Urine Test of Urea-to-Creatinine Ratio," *Advanced Biomedical Engineering*, vol. 7, pp. 72-81, 2018.

Here, over 10 separate experiments were designed to replicate the results of Suzuki et al, however the high absorbance of water above 1600-nm proved to make resolving minute changes in absorbance statistically flawed. A Lambda 950 spectrometer was used (described more in section 4.3), with varying system parameters and different supplementary equipment; nevertheless, the curves in Figure 3-7 were far from being replicated. Appendix A illustrates some of the basic data retrieved from these experiments; the goal of displaying these being to help guide future prospects into the NIR detection of creatinine.

With the NIR range not being viable, effort was shifted towards the UV-VIS range, guided minimally by an older publication in the *Clinica Chimica Acta: Simple and Accurate Method for the Determination of Creatine and Creatinine*. This work by B.L. Dunicz is an aside to the Jaffe method mentioned in the beginning of this paper, as it involves the reaction of creatinine with an alkaline picrate reagent in solution to form a colorimetrically-detectable weak bonding structure [40]. The resulting absorbance peaks are present between ~200-nm and 300-nm (no permission to display their figures). Beer's law (Equation 4)

dictates the linear relationship between absorbance (A) and concentration of the solute (c), which would be elucidated from experimentally calculating a reference curve [41]. Below, 'b' refers to the path length (a quality of the corvette used), and epsilon refers to the absorptivity (of creatinine in this case). Note that Beer's law is a first order approximation, meaning that the linearity of the relationships are better kept when a smaller range of concentrations are imposed.

$$A = bce \quad (4)$$

It is hypothesized that introducing picrate is not necessary to detect dissolved creatinine in this range; this is because creatinine has two local peaks in the 200-300nm range, and because Dunicz noted in his publication that the picrate is used to "amplify" a signal (possibly by increasing absorptivity). Hence, with properly calibrated and sensitive equipment, the presence of creatinine in solution is likely possible. The experimental plan which ultimately yielded viable results is relayed below in section 5.3 "Reference Curve."

3.4 SCATCHARD ANALYSIS

The goal of section 3.3 was to demonstrate a reliable method for determining changes in creatinine concentration in solution, such that a Scatchard analysis can be performed—this is the method used for characterizing the binding parameters of the MIP. A Scatchard analysis is a typical test for a ligand-receptor system (a.k.a. antigen-antibody system), which is adapted to fit the principle of an MIP.

These binding characteristics come in the form of Q_{\max} and K_d . Q_{\max} is the approximated saturation value for maximum number of ligand binding sites on the receptor, which for an MIP is the number of usable

template binding sites per gram of polymer material (“ligand” and “template” are analogous here). The goal would be to maximize Q_{max} , relative to the value calculated for the NIP. The dissociation constant K_d is an equilibrium constant which describes the propensity of the ligand to bind to the receptor/MIP when exposed, typically via a liquid solution [26]. K_d also affects MIP characteristics; a low binding capacity means that a steep concentration of free creatinine would be needed to fully populate the MIP, for example.

These parameters are elucidated via a simple experiment which involves exposing MIP and NIP samples to different concentration solutions of creatinine and calculating the amount of creatinine lost to the polymers during exposure. The governing Equation 5 of the Scatchard analysis is as follows:

$$\frac{\bar{Q}}{[L]} = (Q_{max} - \bar{Q})/K_d \quad (5)$$

Where \bar{Q} is the average number of ligands bound to a receptor, which is represented as the bound mass of creatinine divided by the mass of polymer, and therefore is an input to the equation. $[L]$ is another input; it is the solution concentration of the ligand, creatinine. Again, Q_{max} is the saturated binding capacity for the MIP, which is approximated via the above equation as the x-intercept. K_d in this equation is the negative reciprocal of the linear slope (Equation 6) [42].

$$K_d = -1/m \quad (6)$$

Miura's group determined that for the MIP, there showed to be two sets of binding sites: high and low affinity. For the high affinity, Q_{max} and K_d were found to be $1.3 \cdot 10^{-5}$ mol/g and $7.5 \cdot 10^{-5}$ mol/L, respectively. For the low affinity sites, Q_{max} and K_d were $1.8 \cdot 10^{-5}$ mol/g and $1.8 \cdot 10^{-4}$ mol/L, respectively. For the NIP, Q_{max} and K_d were $1.3 \cdot 10^{-5}$ mol/g and $1.7 \cdot 10^{-4}$, respectively.

Section 5.4 will describe how this experiment is carried out. Overall, the Scatchard analysis is essential to verifying the binding characteristic function of the MIP, which should be specific and sensitive to creatinine in comparison to its non-imprinted variant, the NIP.

4 EXPERIMENTAL SETUP

This section details the preparation setups for synthesizing the imprinted polymers and analyzing creatinine solutions in order to characterize polymers via the theory provided in section 3.2. All appropriate glassware if not specified otherwise was decontaminated via ethanol and dried in an oven.

4.1 POLYMER SOLVENT PREPARATION

Solvents used in the polymerization process are degassed to void the reaction environment of as much oxygen as possible. Oxygen is known to react with free radicals which alters polymerizations kinetics and possible the resulting polydispersion, which is undesirable for standardization and the stability of the polymer products [43].

To extract the oxygen, a freeze-pump-thaw cycle will be utilized twice for each solvent: acetonitrile, toluene, MAA, divinylbenzene (DVB), and the aqueous creatinine solution (not present in the NIP control).

All these reagents were sourced from Sigma Aldrich (St. Louis, MO, USA). The procedure used closely follows the steps outlined by Sarah Miller in “Tips and Tricks for the Lab: Air-Sensitive Techniques,” but to Summarize: each solvent was frozen using liquid nitrogen, then attached to a Schlenk line (Figure 4-1) to have its headspace evacuated. The Schlenk tubes were then re-sealed and allowed to thaw, at which point trapped gasses in the solvents would enter the vacuumed headspace. This process was then repeated for a total of two cycles per solvent, in order to minimize the oxygen present during synthesis. As recommended the solvents were used within three days of degassing (sealed until use) [44].

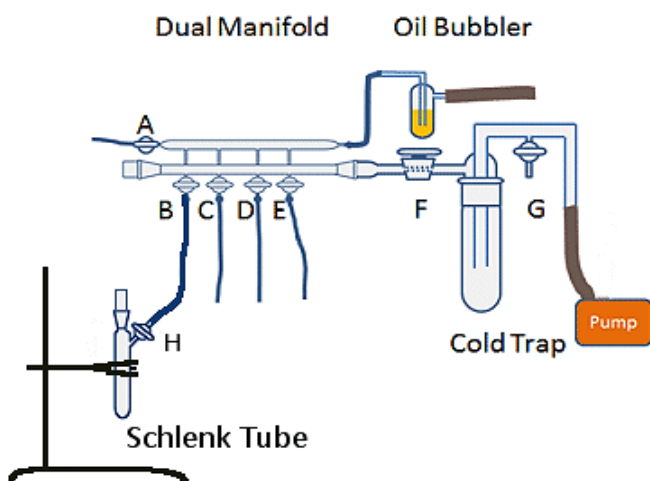


Figure 4-1. Schlenk line apparatus for freeze-pump-thaw degassing method [44].

4.2 SYNTHESIS APPARATUS

This creatinine MIP polymer is synthesized using precipitation polymerization to yield microbeads, a fine white powder which will hold its shape if packed. This flask-contained reaction requires a steady heat source, cooling of evaporated compounds, and sustainment of an inert atmospheric headspace throughout the synthesis.

To fulfill these requirements, the following apparatus was assembled in a chemical hood (Figure 4-2, Figure 4-3). To Summarize: a 3-neck flask was submerged in a silicon oil bath on top of a hotplate; just enough to submerge the reacting solution inside. The hotplate would provide controlled heat and stirring capability to the reaction and was temperature-controlled via a thermistor rod placed in the silicon oil. Connected to one neck was a Liebig condenser which was provided cool water to help condense evaporated solvents. Another neck was used to slowly perfuse the headspace with pure nitrogen gas, which also contained a small exhaust port to prevent over-pressurizing. The third neck was sealed during synthesis.

Section 5.1 will detail how this setup was used to form molecular imprinted polymers via precipitation polymerization.

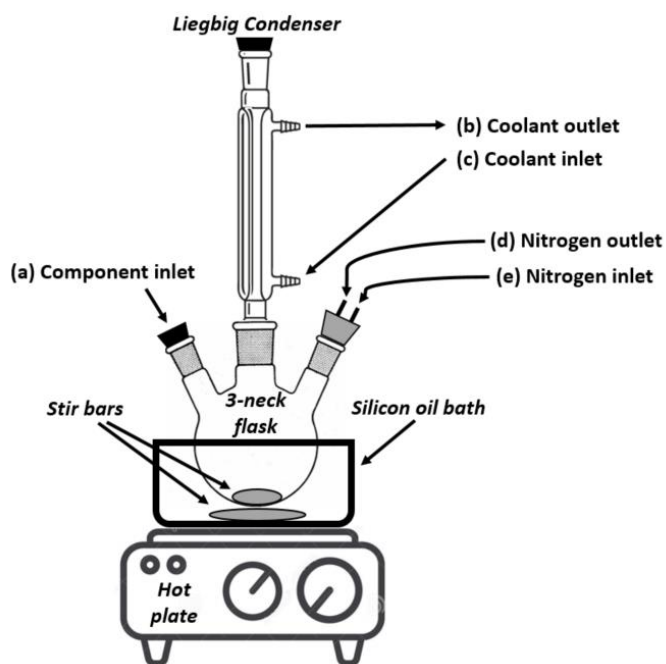


Figure 4-2. MIP synthesis apparatus diagram. Atop a hotplate is a silicon oil bath in which a 3-neck flask was submerged in to control synthesis temperature. Stir bars are placed in both the oil and flask to promote homogeneity. The left neck of the flask

(a) was only used to dispense reaction components and was sealed off during synthesis. The top neck housed a Liebig condenser, which was provided cool water (b,c) to help condense evaporated solvents. The right neck was used to perfuse the headspace with pure nitrogen gas (d,e) to prevent undesired reactions with oxygen molecules.



Figure 4-3. MIP synthesis apparatus photograph.

4.3 UV-VIS SETUP

With the need for solution-based creatinine sensing establish and with some guidance from Dunicz's publication, (see section 3.3), a general setup for utilizing UV-VIS on purified aqueous solutions containing varying amounts of creatinine has been formulated such to relate absorbance to creatinine concentration. A Lambda 950 spectrometer (PerkinElmer Inc.) with a single-cell holder sufficed in capturing a sufficient wavelength range for determining creatinine presence (Figure 4-4). A glass cuvette with a 10-mm path

length and ~4-mL fill volume was used to hold each sample. Controlled by the UV WinLab software (PerkinElmer Inc.), the spectrometer would cycle through the wavelength range multiple times for averaging purposes. The slit width was fixed at 2.0-nm, and the CBM fixed at 100% for all runs. The following sections 5.3 and 5.4 go into further detail about the parameters of each unique experiment.



Figure 4-4. Lambda 950 spectrometer.

5 EXPERIMENTAL PLAN

Sections 5.1 through 5.4 loosely follow two recent publications out of the School of Pharmacy and Pharmaceutical Sciences at the Mukogawa Women's University in Japan [5] [6]. The group details the procedure for synthesizing and purifying a proof-of-concept molecularly imprinted polymer for creatinine using precipitation polymerization, then evaluating the MIP for the aforementioned functional qualities of an imprinted polymer via reference curves, chromatographic evaluation, and a Scatchard analysis. Instead of chromatography, the use of UV-VIS spectroscopy for polymer characterization will be evaluated. Note that there is no experimental plan for section 7 "Results and Discussion: Polymer Characterization"; the procedure used for collecting Raman spectra and SEM images is non-unique.

5.1 POLYMER SYNTHESIS

The objective here is to synthesize polymer microbeads using precipitation polymerization, a process which elicits better control over the resulting polymer molecular weight distribution (MWD) as described in section 3.1.4. The reaction utilizes the apparatus from section 4.2, and requires 24 hours in said vessel under automated heat and stirring control. The *non*-imprinted polymer (NIP) control is synthesized similarly to the *molecularly* imprinted polymer (MIP), but does not include the aqueous creatinine solution, and hence the two procedures will be combined to one below.

To begin the experiment, the synthesis apparatus described in section 4.2 was flooded with nitrogen gas a very low rate (such to not let too much evaporated solvent escape). Next the reagents in Table 5-1 below were relieved from their sealed Schlenk flask after being degassed (see section 4.1) and added to the synthesis flask in the following respective order. All reagents were sourced from Sigma Aldrich (St. Louis, MO), and water was purified via a Millipore Direct Q3.

Table 5-1. Reagents used to synthesize the MIP and NIP.

Reagent	Function	Quantity	Source	Mixing Order
Acetonitrile	Solvent	96-mL	Sigma Aldrich	1
Toluene	Solvent	32-mL	Sigma Aldrich	2
Methacrylic acid	Functional monomer	0.601 grams	Sigma Aldrich	3
Creatinine Anhydrous	Template	9.7-mg in 4-mL H ₂ O	Sigma Aldrich	4
Divinylbenzene	Crosslinker	3.75 grams	Sigma Aldrich	5
AIBN	Initiator	0.314 grams	Sigma Aldrich	6

Miura et al utilized a 128-mL mix of acetonitrile and toluene, and provided the amounts of other reagents in millimole, which here is translated to grams to provide a measurable value. Mass values also helps predict that the resulting MIP/NIP products should each be in the 4 to 5-gram range. At this time, stirring via stir bars placed in the silicon oil bath and the synthesis flask began stirring at about 30 rpm for the entirety of the process. The hot plate began heating to 60 Celsius where it remained, feedback-controlled via a thermistor suspended in the silicon bath. Synthesis took place in a controlled fume hood for 48 hours under these conditions for both the MIP and NIP on separate occasions.

After 48 hours, a fine white powder had precipitated out of solution (Figure 5-1). The entire solution was transferred to another flask for purification, as is detailed in the next section.

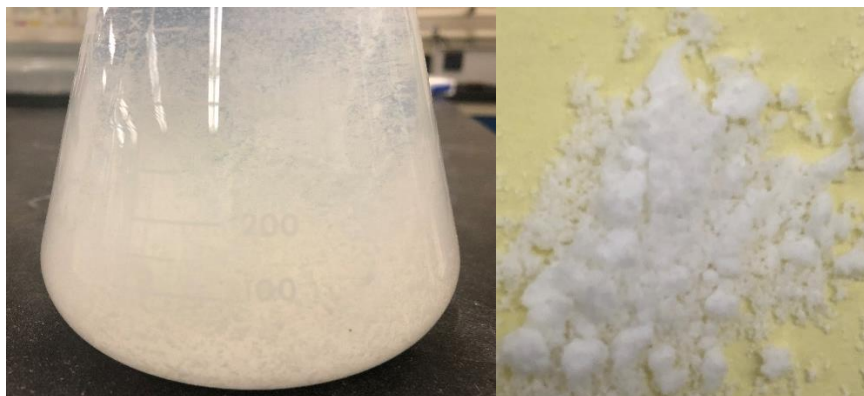


Figure 5-1. Freshly polymerized MIP (left: agitated in solution).

5.1.1 Notes on polymer synthesis

During the first synthesis batch, the nitrogen gas flow through the 3-neck flask proved to be too high, as within 8 hours of beginning the reaction there was no solvent left in the flask—evaporation was constantly occurring, and too quickly. This was amended by minimizing the flow of nitrogen.

As a result of the evaporation issue, the prepared (degassed) reagent supply was exhausted. It was attempted to fabricate an MIP without degassing new reagents, which resulted in a similar microbead powder as expected, but the mass of the powder was about 0.8 grams—about five times lower than the predicted amount, and a cause for suspicion. This is likely a result of free oxygen inhibiting polymerization dynamics, leaving more monomer and/or small polymer nuclei present in the solution, which were likely filtered out during the purification process (described next). All reagents from that point on were degassed via the process outlined in section 4.1.

5.2 POLYMER PURIFICATION

Purification of the MIP refers both to the extraction of the creatinine template, but also the removal of remaining solvent and small polymer chains that would likely not exhibit MIP functionality.

Extraction of creatinine and small, soluble polymer chains involved a vacuum filtration assembly from Sigma Aldrich (Figure 5-2). The synthesis solution is poured into the top, and vacuum is pulled in the bottom flask which draws solution through the 47-mm glass membrane with a 0.45- μm pore size (MIP microbeads are expected to be in the 1-10 micrometer range) [45]. The result is a partially dehydrated powder, which is removed from the filter face and placed in a clean flask. Then, this process was repeated with different 100-mL batches of fresh solvents: three times with methanol (VWR Chemicals, Radnor, PA, USA), followed by twice with purified water, and once with a 50/50 acetonitrile-methanol mix. After solvent addition, the polymer was set in Vortex-Genie 2 vortex mixer for 15 minutes, and then allowed to settle for 2 hours before utilizing the vacuum filter assembly again. The filter membrane was cleaned with methanol between each use.

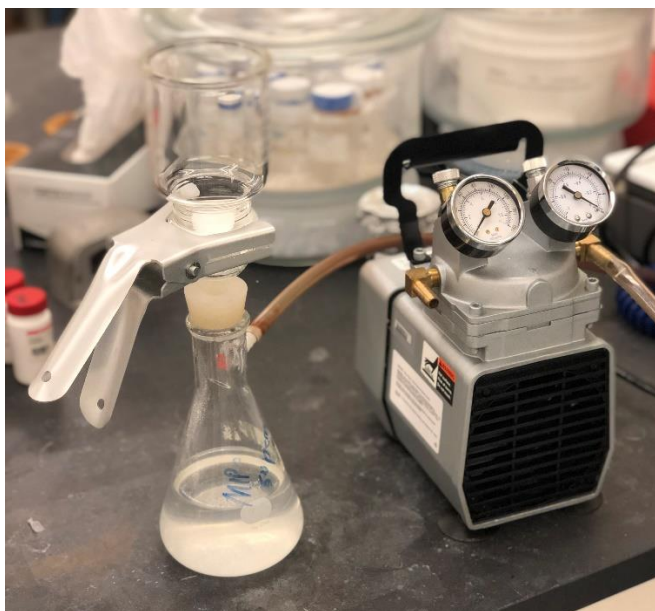


Figure 5-2. Sigma Aldrich vacuum filter assembly with vacuum pump.

After all rinses, the remaining MIP/NIP was dried in a vacuum oven at 45 degrees Celsius for 6 hours. The result was a delicate, chalk-like piece of material with masses of 4.425 and 4.220 grams for the MIP and NIP, respectively (Figure 5-3). Discrepancies in mass are expected because the purification process by principle is used to remove unpolymerized and short-chain polymers from the batches. Nevertheless, to return these products to a more powdery form, the wafer was shaken by hand in a flask. A homogenous powder allows for easier mass measurement, and standardization of the form factor of this material which impacts binding kinetics. Next, SEM and Raman will be used to characterize the produced materials.



Figure 5-3. MIP sample after drying.

5.3 REFERENCE CURVE

The objective of this section is to successfully present an experimental plan for detecting the uptake of creatinine into the MIP material via detecting changes in creatinine solution concentration. See Section 3.3 for the theory behind this necessary experimental step.

The early work of Dunicz provided the wavelength range to begin looking into, and Suzuki et al's publication, while problematic, provided a concentration range that would be both physiologically relevant and detectable using optical methods.

Hence solutions of creatinine were created at 2.5, 5, 7.5, 10, 15, 20, and 500 mg/dL concentrations by first mixing a stock solution of 500 mg/dL, and then following a dilution scheme which is briefed in Appendix B.

To collect the absorbance spectra of each solution, 4.0-mL of each would be pipetted into cuvettes and inserted snugly into the single-cell holder inside the Lambda 950 UV-VIS spectrometer (Figure 4-4). Using the settings specified in section 4.3, the spectrometer would scan through a wavelength range of 240-280

nm in 2.5-nm increments. Each sample was cycled 10 times, one after another, for averaging purposes. Excel files were produced with the resulting absorbance spectra (Figure 5-4). These were inputted into a custom MATLAB script for analysis (see Appendix C). To convert between absorbance and percent transmittance, the following Equation 7 was implemented. Note that absorbance is unit-less, but typically denoted with units AU.

$$\text{Absorbance} = A = \log\left(\frac{100}{\%T}\right) \text{ or } \%T = 100/10^A \quad (7)$$

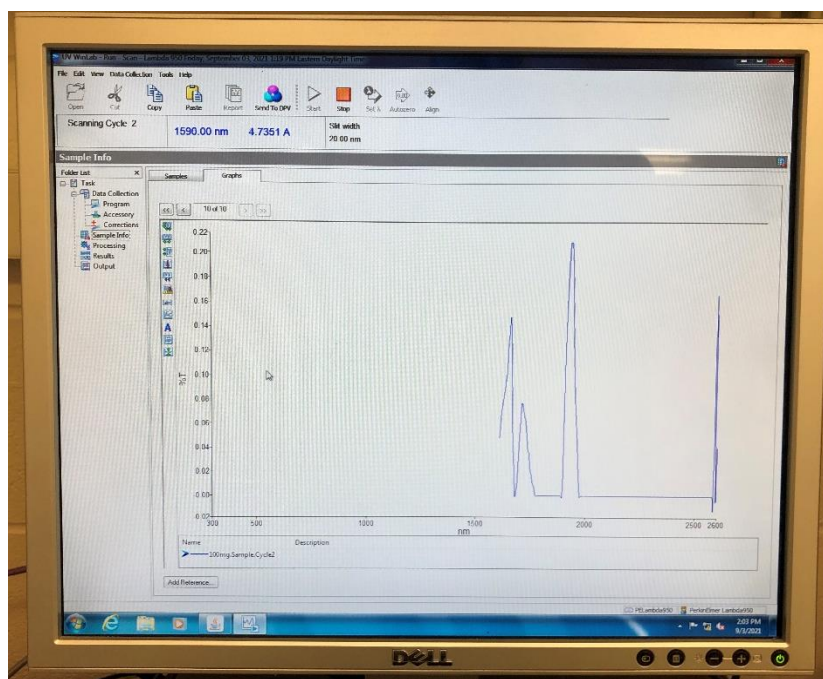


Figure 5-4. View of UV WinLab software mid-capture.

5.4 SCATCHARD ANALYSIS

A Scatchard analysis is performed to deduce binding parameters Q_{\max} and K_d . The premise of the experiment is to put some MIP into a known solution of creatinine, then after some time the pure solvent will be sampled and ran through the spectrometer—and using the results from the reference curve experiment, the new creatinine concentration and therefore the change in dissolved creatinine mass can be calculated. This data will then be relayed in the standard format of the Scatchard analysis (section 7). This section is sequenced chronologically, where there is mention of some of trial and error such to prevent others from making the same mistakes in future works.

For the experiment, the MIP and NIP would be exposed to the same initial creatinine concentrations as in the reference curve experiment (2.5, 5.0, 7.5, 10, 15, and 20 mg/dL). Initially it was planned to have three separate samples at the same creatinine concentration to account for measuring errors; this was later changed to 1 for reasons to be explained.

Hence initially 36 15-mL vials were labeled and filled with 60-mg of the MIP or NIP, followed by 6-mL the respective creatinine solution (Figure 5-5). Vials of just purified water, MIP+H₂O and NIP+H₂O were also made for reference. The creatinine mass and fluid volume values are akin to those used by Miura et al (10-mg and 1-mL), with the larger volumes being necessary to fill the spectrometer cuvette. Following all sample preparation each vial was put on a Vortex-Genie 2 vortex mixer (Scientific Industries), shaken on medium for 30 minutes, followed by a 24-hour rest period. This shaking and rest period was repeated once more. Note that the MIP should not take nearly this long to equilibrate with the creatinine in its environment; these times were just convenient for the user.



Figure 5-5. Vials of creatinine solution containing MIP (“M0”) and NIP (“N0”). Left photo taken after agitating the solution.

Following the final “rest” period of the solutions, it had appeared that both the MIP and NIP (mostly the NIP, see Figure 5-5) had released some colloids, and possibly dissolved particles into the creatinine solution. Whether this is a result of insufficient purification of the polymer (section 5.2) and/or polymer breakdown over time is not known; but these released molecules took about 24 hours to noticeably appear in solution. With hope that the released molecule quantity would be consistent enough between samples, and that their absorbance value, if any, could be subtracted: the spectroscopy procedure was started.

A 3.8-mL aliquot of each solution was collected using a small pipette tip gently inserted towards the bottom of each vial, where the fluid was moved to the spectrometer cuvette. Upon insertion into the spectrometer, the fluid was allowed to settle for two minutes, such that any precipitates that made it into the cuvette could settle such not to disrupt absorbance readings at the set 275-nm value (there was not noticeable precipitate). 30 cycles were collected for each sample for the MIP and NIP at the 2.5, 5, and 7.5 mg/dL concentrations before realizing that the data would not be consistent enough to produce

accurate results. The inconsistencies resulting from the colloidal/dissolved molecule presence was an order of magnitude larger than the changes that would result from a small loss in creatinine concentration (as the polymer bonded the creatinine).

As a result, the experimental plan needed to be altered such to filter out as much colloid presence as possible. To accomplish this, the remaining fluid volumes at each concentration (which account for the decrease of the 3 to 1 sample size) was put into the necessary amount of Nanosep Centrifugal Devices with Omega Membrane (300K) and inserted into an IEC Centra CL2 Centrifuge (Thermo Electron Corporation) for three minutes at 3500-rpm. Note that all the 2.5-mg/dL samples were used up in the first pass. This was done with the three reference samples as well. The resulting filtered fluid appeared as clear as pure water, hence the above procedure was restarted, but with the decrease in sample size.

However, despite the additional precautions, evaluation of the data via a custom MATLAB code determined a very poor correlation between the absorbance and the concentrations of the five MIP samples (Figure 5-6). Absorbance values, when corrected for by the reference MIP sample (60-mg of MIP that was submerged in 6-mL purified water), were on the magnitude of expected absorbance, but slightly higher than could be expected. Absorbance in the UV-VIS range is not as selective as it is in the NIR range; hence a wide range of contaminants could be artificially increasing the absorbance value measured. Possible contaminants include residual creatinine (just in the MIP case), trapped monomer leachates, and any polymer breakdown products resulting from hydrolytic degradation in solution.

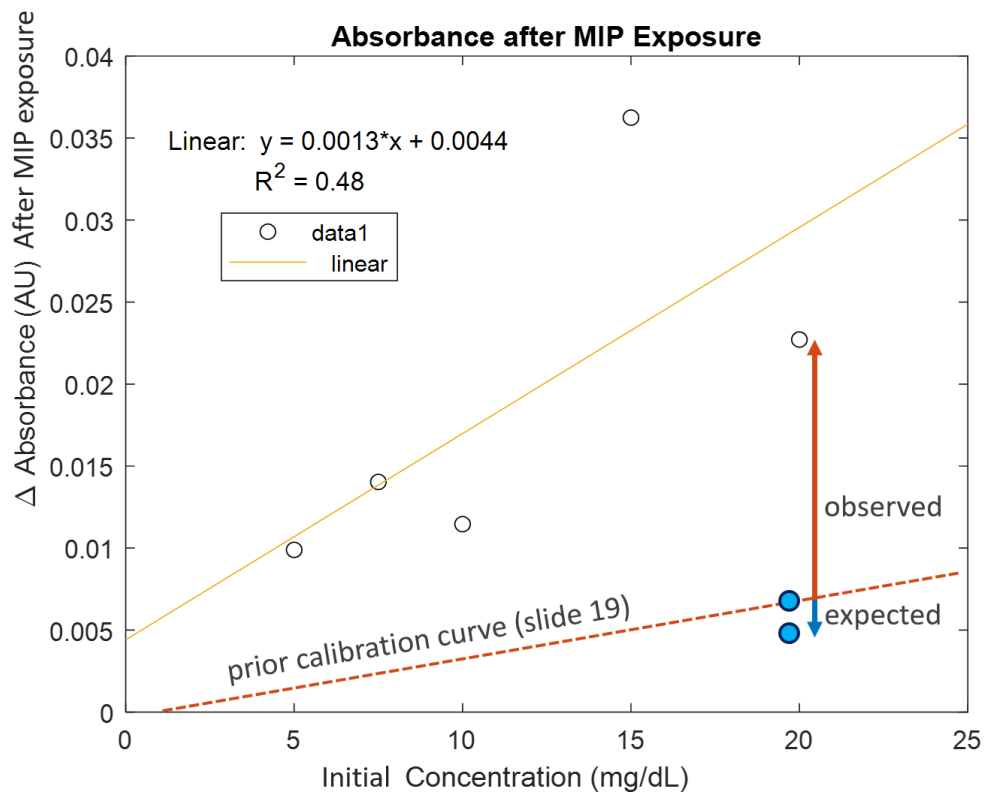


Figure 5-6. Absorbance versus concentration for the purified MIP samples.

With this knowledge it was decided that the experiment would be restarted, but on a smaller scale with additional steps that should deter some of the variance and contaminants associated with the former process.

5.4.1 Refined Scatchard Analysis

To repeat this experiment, it was essential to conserve the remaining MIP/NIP produced, as the variance that could result between different syntheses has not been characterized. Hence, the 20 mg/dL sample set was excluded from the Scatchard analysis (Miura et al only went up to ~ 11.3 mg/dL in the publication) [6].

To further purify the polymers themselves (beyond what is detailed in section 5.2), each remaining batch (~3 grams each) was diluted into 150-mL of a 50:50 v/v solution of water and acetonitrile and then placed onto a vortex mixer for 1 hour. Each solution was then left to rest for 23 hours, before the fluid was extracted using a vacuum filtration assembly with a 0.45- μ m membrane. This process was repeated twice more to ensure removal of possible colloids and dissolved particles. Finally, each polymer was dried in an oven over the course of 3 days at 40°C.

Next, new vials were filled with 45-mg of the MIP and NIP, and 4.5-mL of purified water creatinine solutions for the new Scatchard analysis. To conserve remaining polymer, 3 samples at only 5.0, 7.5, 10, and 15 mg/dL concentrations were prepared. Each vial was vortexed as detailed above, followed by filtration of the resulting solutions through 10K Nanosep Centrifugal Devices (versus 300K devices). The filtered solutions were then run through the spectrometer via the original plan, with the results of said experiment detailed below (section 8).

6 RESULTS AND DISCUSSION: REFERENCE CURVE

This section is split into halves: the former presents the results for the preliminary experimentation with UV-VIS creatinine detection, and the latter presents the optimized method used for the other experiments in this paper.

The custom MATLAB code for the results presented can be found in Appendix C.

6.1 REFERENCE CURVE EXPERIMENTATION

Refining the UV-VIS process to yield consistent and accurate results proved to be a challenge, but ultimately a reproducible reference curve relating the absorbance of creatinine to its concentration was deduced. Determining this curve was essential for proving the concept and allowing some process optimization to occur afterwards.

Foremost, for the sampling outlined in section 5.3, the consistency of the Lambda 950 spectrometer is assessed via the following Figure 6-1 for each of the 7 sample concentrations. Each of the 10 cycles per sample is displayed by black lines, and the average of the cycles is a red line. The spectrometer was highly consistent, with an example standard deviation at 275-nm being displayed on each graph, being on the order of 10^{-5} .

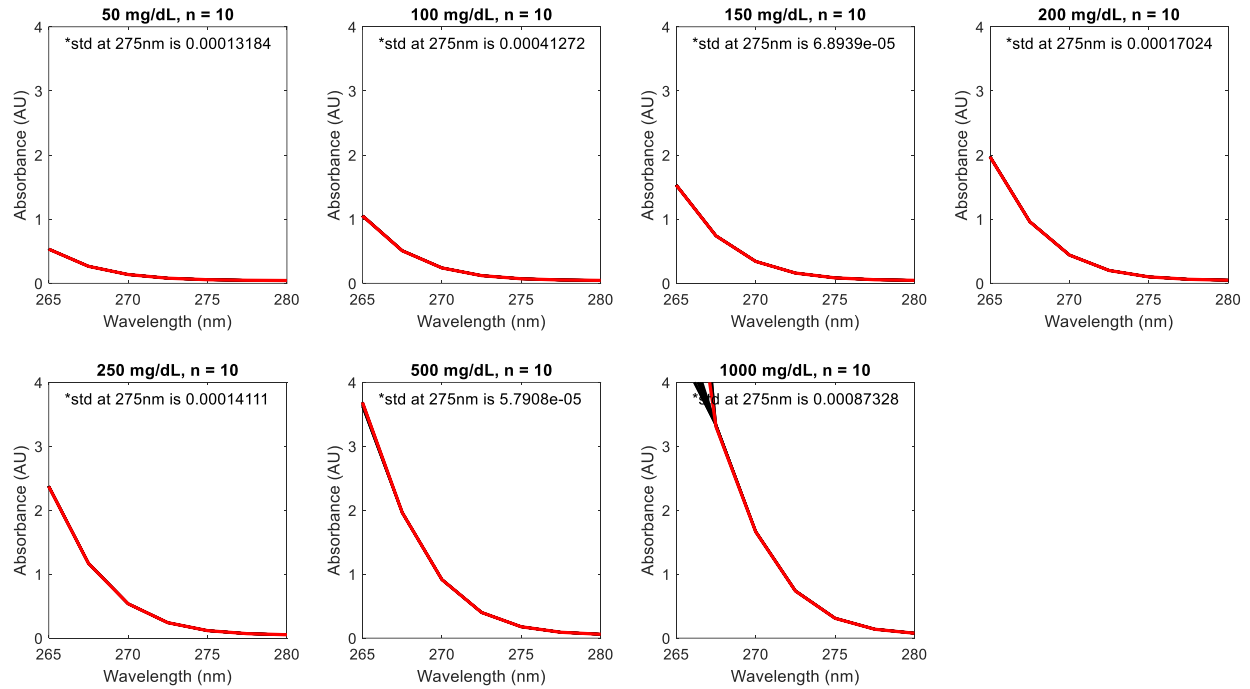


Figure 6-1. All spectrometer spectra w/ averages for reference samples.

Next, each average spectra were compared, both in terms of absorbance and percent transmittance (Figure 6-2). Both means of displaying relative intensity demonstrate a consistent pattern relative to solute concentration. Of note is that data below 250-nm was collected, but there were many absorbance spikes to 10 AU (the max value) that meant that those portions of the data were not viable. It is not suspected that data in those regions would have improved results.

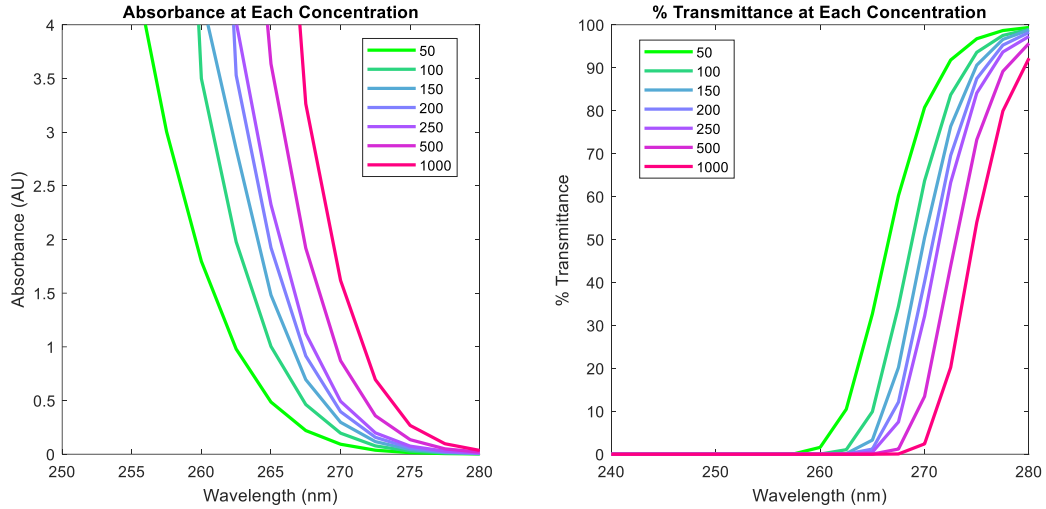


Figure 6-2. Absorbance and % transmittance for reference samples.

Next, as these peaks are broad, the area under each peak between 260 and 280-nm was compared, by programming a Reimann sum across the data points (Figure 6-3). The relationship proved not to be linear for either absorbance or percent transmittance, hence a more direct approach was employed.

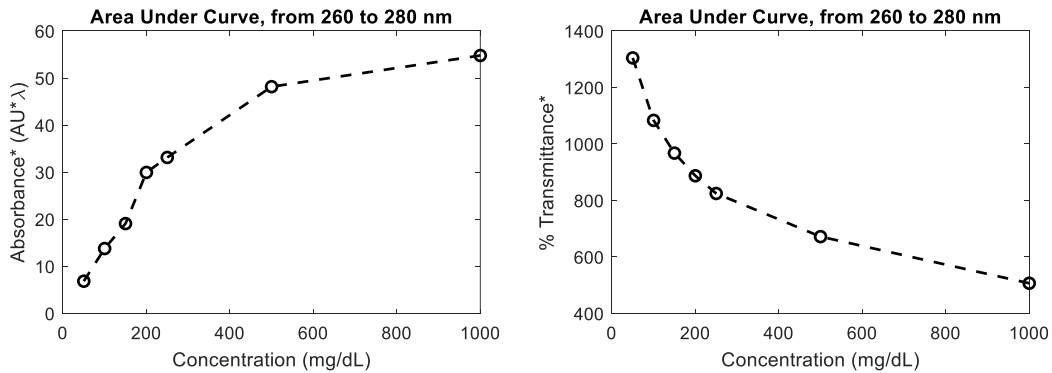


Figure 6-3. Area under curves for section of reference samples spectra.

The final part of the MATLAB code in Appendix C cycles through each set of points for every wavelength, and calculates the correlation coefficient R at each wavelength, then presents the graph for whatever single wavelength yielded the highest R² value. The strongest correlation was at 275nm, with an R² equal to 0.999 out to three digits (Figure 6-4). R² values at neighboring 272.5 and 275.5-nm were greater than 0.98, demonstrating the possibility that a wider observation range could improve results. Nevertheless, the acquired curve was well within the realm of accuracy needed, considering the small deviation of the spectrometer and the deviations resulting from diluting the creatinine solutions by hand.

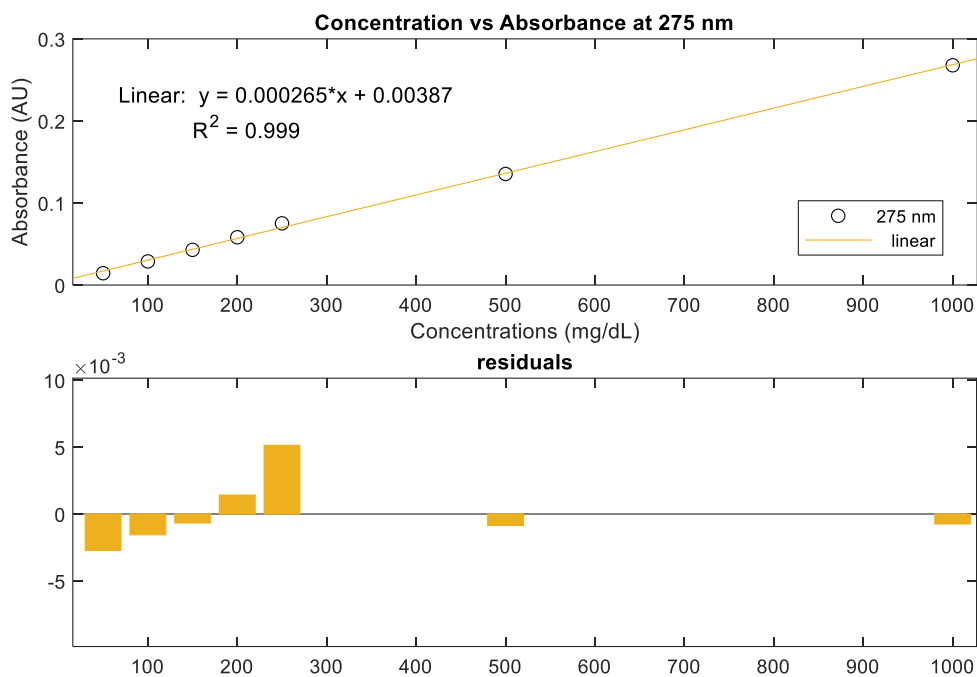


Figure 6-4. Preliminary reference curve and respective residuals.

Therefore, the following Equation 8 can transmute the concentration of a creatinine solution to its absorbance value and vice versa:

$$A = 0.000265c + 0.00387, \text{ or } c = (A - 0.00387)/0.000265 \quad (8)$$

Where A is the absorbance and c is the solution concentration of creatinine. The residuals of this curve point to a downfall of Beer's law: that it is only an approximation, and therefore more accurate as the concentration range shrinks [41]. Nevertheless, a sufficient linear relationship combined with the single-wavelength observation increased the efficiency of future sampling via only needing to sample at 275-nm; and this discovery offers the possibility of a single-wavelength LED to be used for emission instead of a whole spectrometer in future works.

These results were verified by re-running the experiment twice with altered creatinine concentrations; with results for the slope of the reference curve never deviating by more than 3.1%, and the offset never deviating by more than 0.002 AU.

Considering the consistency of the results, it was theorized that only the absorbance value at 275-nm was needed for future measurement of creatinine concentration. Verifying this hypothesis would improve computational and time efficiency of all future data collection and analysis. Secondly, while the concentration range used did produce a linear reference curve, the concentrations were both higher and wider in range than they needed to be for the following Scatchard analysis (if it were to replicate the works of Miura et al) [6]. Hence, a lower concentration range would be investigated too.

6.2 REFERENCE CURVE FINALIZATION

From the prior section, it is noted that only data collection at only 275-nm may be sufficient in determining creatinine concentration. The newer samples included concentrations at 2.5, 5.0, 7.5, 10, 15, and 20 mg/dL. Similarly, each sample was cycled through the spectrometer 20 times for averaging purposes. The

following boxplot demonstrates the variance at each concentration (Figure 6-5); note that the x-axis is not to scale. The Δ in the y-axis refers to the fact that the absorbance for water was subtracted.

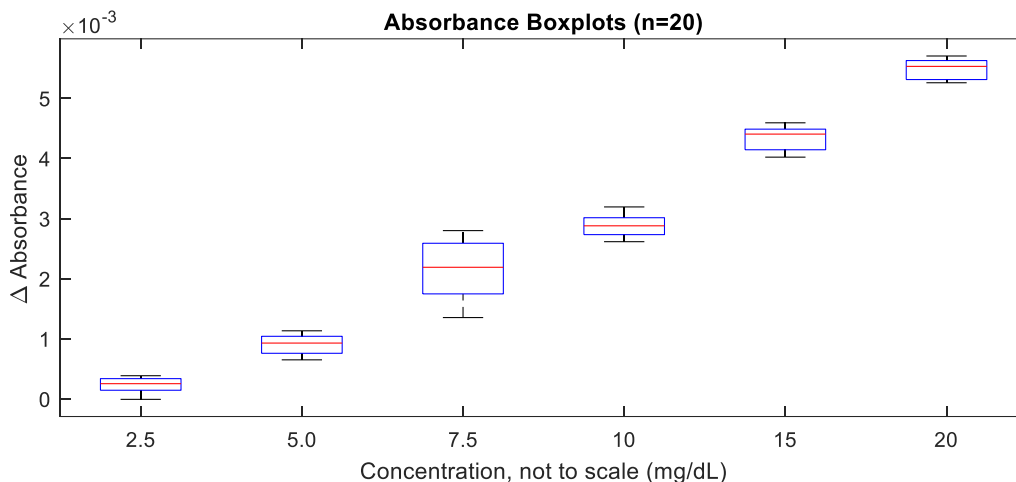


Figure 6-5. Reference curve boxplot.

This boxplot demonstrates that there were no outliers, and that there are no instances where the same absorbance value was measured at different concentrations (no crossover). To get a better idea of how the 20 cycles impacted the data accuracy, the following chart comparing percent deviation from the overall mean as a function of sample number (1 through 20) is shown below (Figure 6-6). Note that the vertical blue bars represent the standard error about the mean at each point. A standard error within 1% is sufficient, but number of cycles was increased to 30 for all subsequent tests to try to reduce this variability further, as the increase in computational cost is negligible. Additionally, it is important to note there is no drift as more samples were taken, which could arise given something in the environment or sample chamber was changing during the scans.

Next, the values were averaged and plotted against the scale concentrations (Figure 6-7).

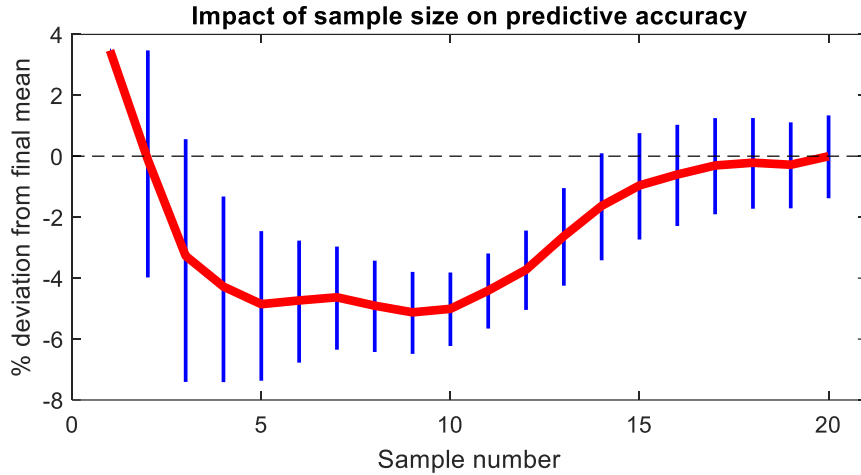


Figure 6-6. Impact of sample size on predictive accuracy.

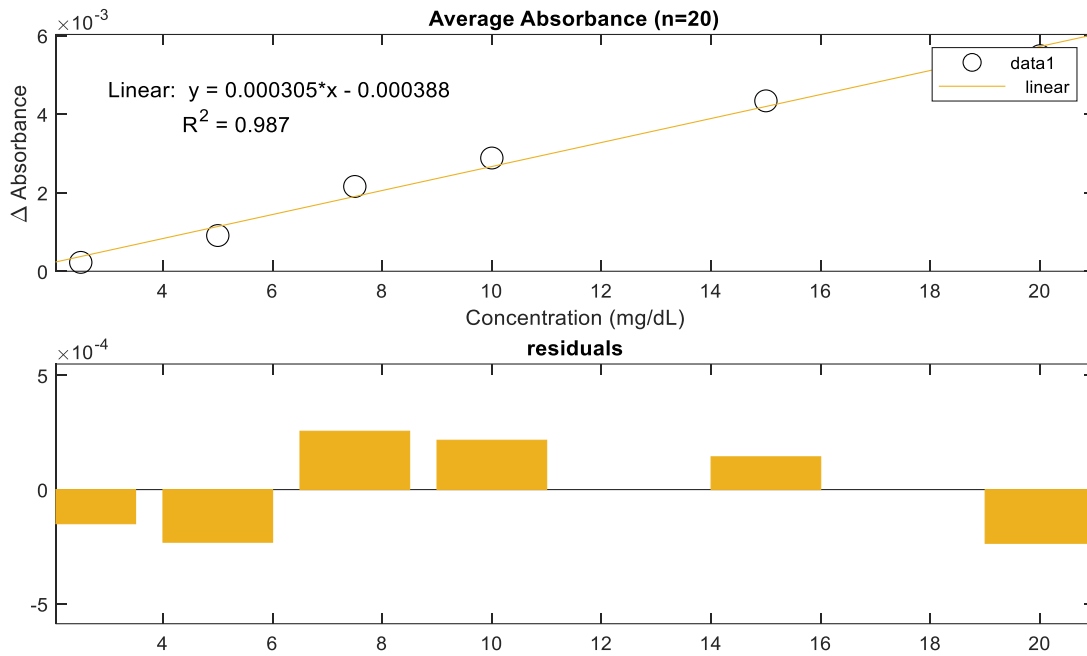


Figure 6-7. Final reference curve.

From Figure 6-7, there is a clear linear relationship between absorbance and concentration of creatinine. The R^2 value is 0.987, which is lower than the value from the preliminary reference curve. This is expected, as when trying to resolve smaller changes in absorbance, the signal-to-noise ratio decreases. This is

countered in future runs by increasing the sample size to n=30 per sample (increasing this value negligibly changes computational effort). Nevertheless, the following Equation 9 is employed for the subsequent Scatchard and temperature-dependence data analyses.

$$A = 0.000305c - 0.000388, \text{ or } c = (A + 0.000388)/0.000305 \quad (9)$$

7 RESULTS AND DISCUSSION: POLYMER CHARACTERIZATION

Any new material can be characterized in a wide variety of ways; while the focus of this paper is on creatinine dynamics of the MIP, presented here is Raman spectra and SEM images for the synthesized MIP and NIP.

7.1 RAMAN SPECTRA

Raman was performed on both polymer variants alongside creatinine powder, which allows investigation of two comparisons: the first is peaks that are common between only creatinine and the MIP, signifying the presence of residual creatinine in the synthesized polymer. The second is peaks that are common between only the MIP & NIP, which demonstrate the common polymer structure of the two variants. The following plots were generated in MATLAB (Figure 7-1). Orange lines spanning subplots indicate common peaks, which are labeled by the assumed vibrational mode(s) at said frequencies.

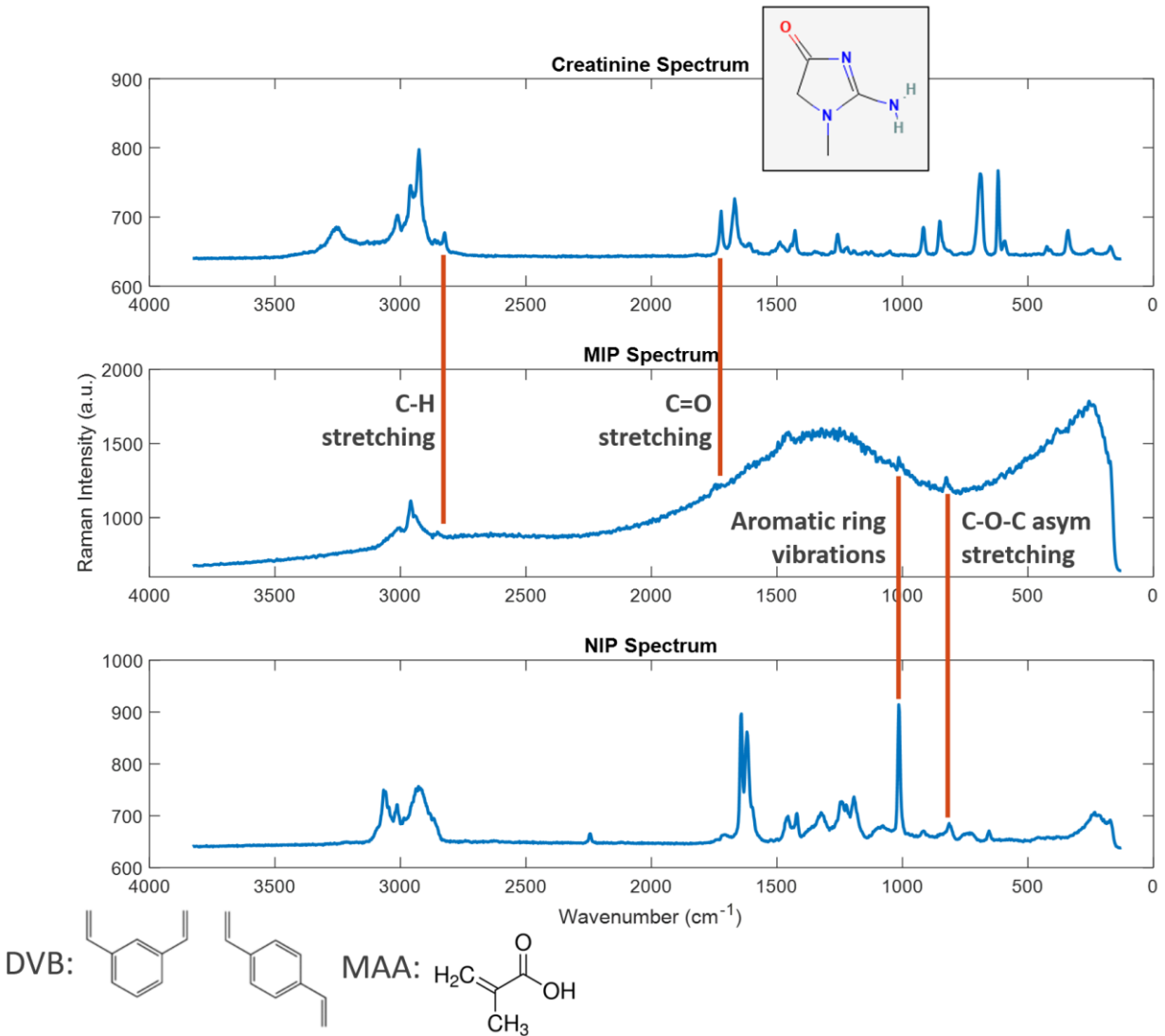


Figure 7-1. Raman spectra for MIP, NIP, and creatinine samples.

From the data, it is foremost apparent that there is the large discrepancy between the MIP and NIP samples, despite their supposed similar chemistry. It is not believed to be an error in sampling, but more samples should be collected to confirm this phenomenon. This fundamental difference is correlated by the SEM data which follows this section. Nevertheless, there are two discernable peaks shared between MIP and NIP structures; at about 1000- cm^{-1} there is a large peak indicative of aromatic ring vibrations; evidently from the aromatic ring in the divinylbenzene crosslinker (DVB's structure is shown in Figure 7-1).

The other common peak about $\sim 820\text{-cm}^{-1}$ is the stretching of asymmetric C-O-C bonds, which are present in methacrylic acid monomer; the asymmetry coming from the occurrence of a double-bonded oxygen on one of MAA's carbons [46].

Unique to creatinine and the MIP was a peak at $\sim 2850\text{-cm}^{-1}$, which could be either the bond stretching between C-H or C-N; C-H bond stretching happens over many frequencies (hence the many common peaks about 3000-cm^{-1} , so it is difficult to differentiate the two using this method [46]. Overall, the uniqueness of the MIP spectrum relative to the NIP was unexpected and makes further analysis difficult, hence this topic should be reevaluated in future works.

7.2 SEM IMAGES

SEM images relayed a similar narrative as the Raman spectra, with the NIP samples presenting a much more believable microstructure relative to the images from Miura et al (Figure 7-2, Figure 7-3, and Figure 7-4). Miura et al achieved polymer microbeads that were about 3.5 and 4.5 micrometers in diameter for the MIP and NIP, respectively (see Figure 3-5). Here, similarly sized microbeads were synthesized for the NIP variant. The MIP, however, expressed a heterogeneous microstructure that was not anticipated. Those images below further bolster the idea that there was an issue during and/or after synthesis that caused this unintended polymer microstructure. Nevertheless, the "micro-flakes" of MIP produced ranged generally from 5-10 micrometers.

Overall, collecting SEM images and visualizing Raman spectra are important steps for material characterization; and what has been done here are initial steps that require further analysis to deduce any hard conclusions about what exactly has been synthesized.

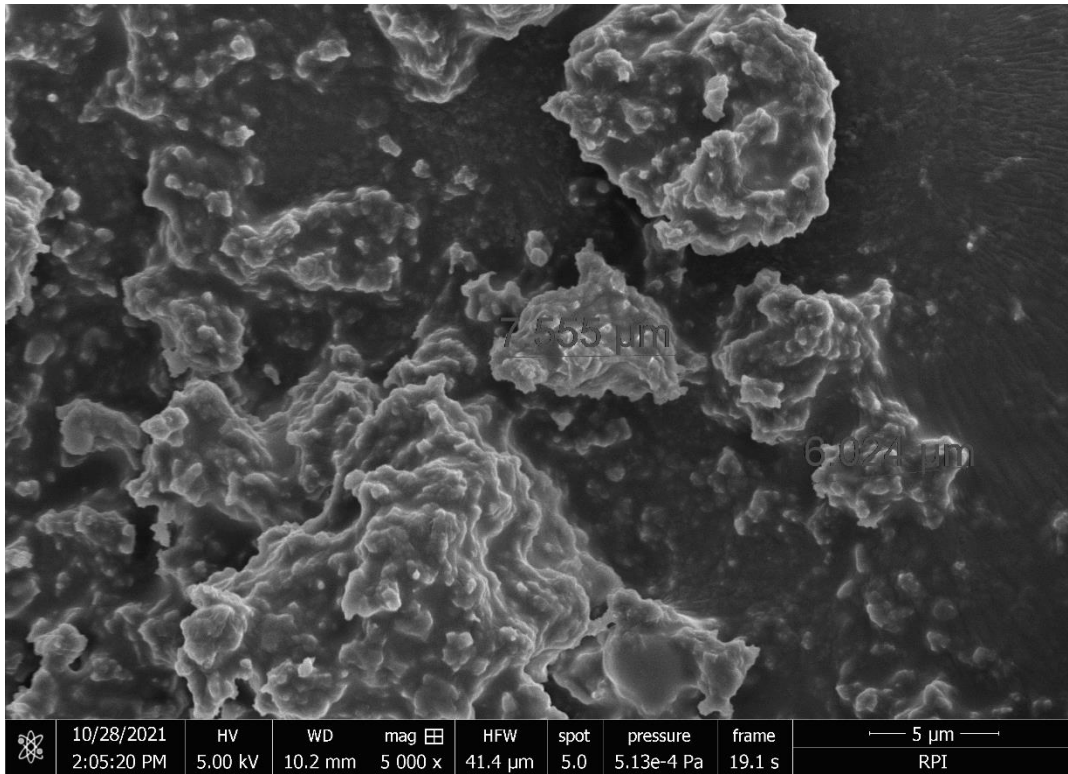


Figure 7-2. SEM image of MIP sample.

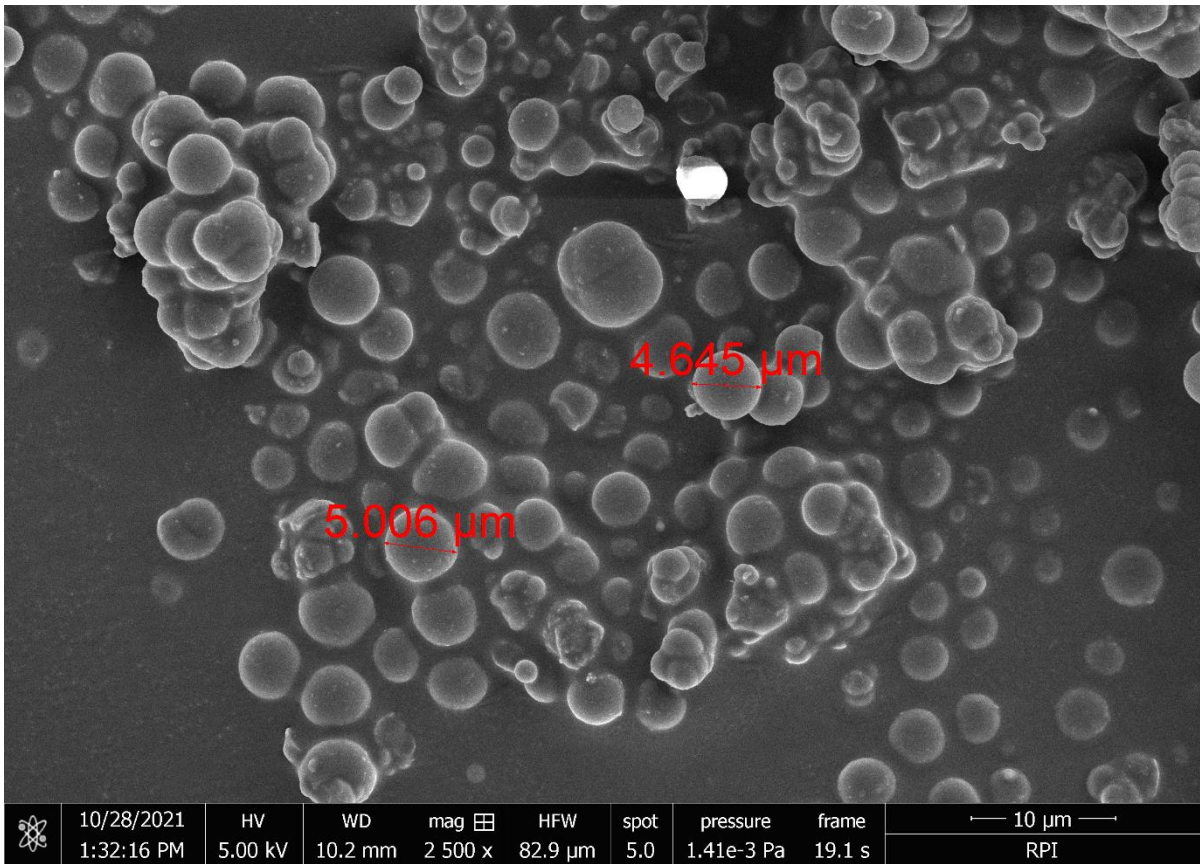


Figure 7-3. SEM image of NIP sample.

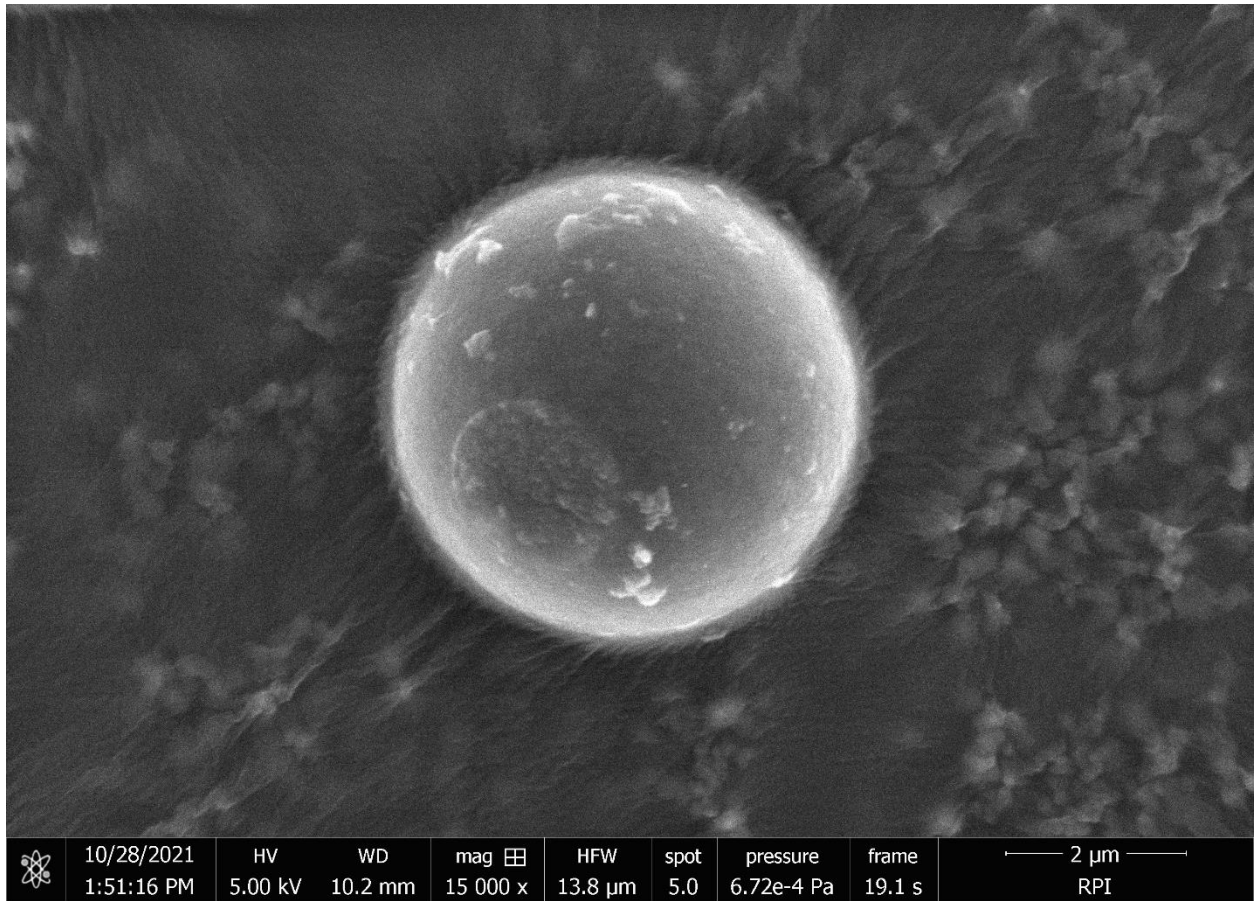


Figure 7-4. Zoomed image of singular NIP microbead.

8 RESULTS AND DISCUSSION: SCATCHARD ANALYSIS

This section details the results of the Scatchard analysis, and how it could be improved in future works.

Unfortunately, the procedure outlined in section 5.4.1, “Refined Scatchard Analysis,” was unable to be completed in due time as a result of malfunction of the spectrometer’s lamp leading to unstable absorbance readings in the desired UV-VIS range. If the data were able to be collected, one would anticipate similar results as are presented in Miura et al’s publication [6]. A MATLAB code is presented in Appendix D that given the proper input file, would output the necessary data and figures for the analysis.

Nevertheless, there are many aspects of the Scatchard procedure which should be optimized for future analysis. Foremost is the MIP/NIP themselves: ensuring fully polymerization (depletion of monomers from solution) is likely to deter from contamination via leftover monomers. Subsequently, promoting aggregation instead of nucleation during synthesis would also deter the presence of non-filterable substrates such as monomers and small nuclei. Balancing aggregation versus nucleation can be executed by varying many parameters including environmental temperature, stirring dynamics, and initiator presence.

Following synthesis, the purification procedure (section 5.2) should be more thorough. Here, polymers were only exposed to pure solvents about 10 times each, the solvent and any residue being filtered through a 0.45- μm vacuum filter. The “soak” time in between cycles is likely longer than it needs to be, and it may promote breakdown through hydrolytic mechanisms when water is a component of the solvent. Hence, utilizing higher acetonitrile-water ratios as solvents may deter degradation, as could decreasing soak times. Additionally, wash cycles could be done rapidly by leaving the polymer on a filter membrane, and continuously flushing large volumes of water through the mixture and into a drain.

Complete, but not harmful, drying should also be ensured. This was not difficult; the polymers turned into a very fine, homogenous powder when fully dry.

As for the samples in the Scatchard analysis, similar rules apply as to what is described above. For the analysis, polymer samples were put in water solutions containing creatinine, shaken, and let rest of the course of about 24 hours. While ensuring full absorption of the creatinine into the polymer is essential for the Scatchard analysis, standard response times for MIP range from seconds to minutes (the disparity resulting from the many form factors of the material) [21]. Hence, it would be efficient to assume that the creatinine has equilibrated by 1 hour after exposure; shortening this time would hopefully deter any degradation products that may arise.

Before spectroscopy, each sample in the Scatchard analysis was aliquoted and filtered using Nanosep centrifuge vials. While their 10K product should deter passage of any polymer chains, monomers and small nuclei may not be filtered out. If assuming that there will always be some level of polymer contaminant, this may be calculated and corrected for if the contaminant presents an absorbance peak in an appropriate range. This range should be predictable based on the functional groups and vibrational modes of the monomers, methacrylic acid and divinylbenzene. Hypothetically discretizing contaminant and creatinine presence in solutions would be difficult solely in the UV-VIS range, because both sources are essentially organic molecules and contain similar groups of atoms.

This concludes the possible improvements to the Scatchard analysis. In conclusion, the MIP and NIP synthesized proved to be a difficult source of contamination to correct for, but with proper protocols spectroscopy may still be a viable alternative to chromatography for characterizing these novel polymer structures.

9 CONCLUSION AND FUTURE WORK

This research into molecularly imprinted polymers has demonstrated a shallower yet wide in breadth approach to begin the characterization of a creatinine MIP beyond the works of Miura et al's group. Synthesis of the material proved sensitive to environmental conditions, and thorough purification of the material after synthesis was determined to be essential if spectroscopy is to be used to characterize the material. SEM images and Raman spectra provide insight into the microstructures and nanostructures, respectively.

Hence there is a variety of directions in which this research could be directed. Foremost, the Scatchard analysis remained in limbo after malfunction with the spectrometer; being able to run those samples and elucidating creatinine binding characteristics Q_{\max} and k_d would be a huge step forward in validating the sensitivity of the polymer as a sensing element. With reference to using spectroscopy, there also exists the possibility that using different detection methods for creatinine in solution such as NMR may be a more precise and selective means of determining unknown concentrations.

Beyond the Scatchard analysis, there are other binding experiments that should be conducted, including ones to characterize response times (how long does it take creatinine to equilibrate with the material) and the dependence of binding dynamics on temperature. These two experiments would be aided by further analysis into SEM and Raman spectra. SEM helps deduce microstructure properties, which effect the mobility of creatinine and therefore the response time. Raman spectra could be used to determine the presence and prevalence of the hydrogen and Van der Waal's bonding that binds creatinine in its template regions; this information would then be used to determine the effects of temperature/pressure on binding dynamics.

Any future experiment on this material should be towards proving the polymer as a stable, sensitive, selective, and cost-effective alternative to organic elements for sensing creatinine presence in urine and blood serum. As noted earlier, this information is vital for calculating glomerular filtration rate, *the proxy*

for renal health. With this data, those 15% of our population who have evolving chronic kidney disease may have a brighter future, as frequent, quantitative patient data would be used to better allot the scarce resources used to currently treat this disease (transplant organ and dialysis machines). MIPs for other biological compounds have just begun their inception into the commercial realm and are beginning to improve global healthcare outcomes for various diseases, conditions, and other non-clinical applications.

10 REFERENCES

- [1] "Kidney Disease Statistics for the United States | NIDDK," National Institute of Diabetes and Digestive and Kidney Diseases, 2021. [Online]. Available: <https://www.niddk.nih.gov/health-information/health-statistics/kidney-disease>. [Accessed 2 June 2021].
- [2] H. Ritchie and M. Roser, "Age Structure," Our World In Data, September 2019. [Online]. Available: <https://ourworldindata.org/age-structure>. [Accessed 3 Sept. 2021].
- [3] M. J. Webb, "Healio," 20 April 2020. [Online]. Available: <https://www.healio.com/news/nephrology/20200420/fresenius-baxter-act-on-national-dialysis-machine-supply-shortage-during-covid19-pandemic>. [Accessed 1 Sept. 2021].
- [4] A. Tena and S. McArdel, *Limited organ availability.*, 2018.
- [5] J. Haginaka, C. Miura, N. Funaya and H. Matsunaga, "Monodispersed Molecularly Imprinted Polymer for Creatinine by Modified Precipitation Polymerization," *Anal Sci*, vol. 28, no. 4, pp. 315-317, 2021.
- [6] C. Miura, N. Funaya, H. Matsunaga and J. Haginaka, "Monodisperse, molecularly imprinted polymers for creatinine by modified precipitation polymerization and their applications to creatinine assays for human serum and urine," *J Pharmaceut Biomed*, vol. 85, pp. 288-294, 2013.
- [7] M. Wilson, "Laboratory Diagnosis of Malaria: Conventional and Rapid Diagnostic Methods," *Arch Pathol Lab Med*, vol. 137, no. 6, pp. 805-811, 2013.
- [8] T. Mandelbaum, "Outcome of critically ill patients with acute kidney injury using the Acute Kidney Injury Network criteria," *Crit Care Med*, vol. 39, no. 12, pp. 2659-2664, 2011.
- [9] "Creatinine," Kidney.org, 2020. [Online]. Available: <https://www.kidney.org/atoz/content/what-creatinine>. [Accessed 23 June 2021].
- [10] "Renal & Urology News," Kidney Anatomy, 2017. [Online]. [Accessed 15 June 2021].
- [11] N. Ahmed, *Clinical Biochemistry*, New York: Oxford University Press., 2011, p. p. 72.
- [12] T. E. Howard, in *Clinical Chemistry*, New York, John Wiley and Sons., 1989, pp. 58-62.
- [13] J. Delanghe, "ANALYTICAL AND CLINICAL EFFECTS OF CREATININE STANDARDISATION," 28 11 2014. [Online]. Available: <https://www.slideserve.com/quamar-barker/analytical-and-clinical-effects-of-creatinine-standardisation>. [Accessed 20 July 2021].

- [14] "Future of Medical Diagnosis | Going Molecular | Insights Care," Insights Care, 2021. [Online]. Available: <https://insightscare.com/future-medical-diagnosis-going-molecular/>. [Accessed 21 June 2021].
- [15] A. Folch, Introduction to bioMEMS, Boca Raton: CRC Press, 2013.
- [16] "Games Proteins Play," FunSize Physics, 2017. [Online]. [Accessed 15 July 2021].
- [17] "Bovine Creatinine Quant ELISA Kit | Competitive EIA | LSBio," Lsbio.com, 2021. [Online]. Available: <https://www.lsbio.com/elisakits/bovine-creatinine-competitive-eia-elisa-kit-ls-f32259/32259?trid=247>. [Accessed 24 July 2021].
- [18] "Stat Profile Prime Plus® Critical Care Analyzer," Novabiomedical.com, 2021. [Online]. Available: <https://www.novabiomedical.com/prime-plus/index.php>. [Accessed 3 Aug. 2021].
- [19] "iohexol," Wikidata.org, 2020. [Online]. Available: <https://www.wikidata.org/wiki/Q410683>. [Accessed 3 Aug. 2021].
- [20] "Inulin," Pubchem.ncbi.nlm.nih.gov, 2021. [Online]. Available: <https://pubchem.ncbi.nlm.nih.gov/compound/Inulin#section=2D-Structure>. [Accessed 3 Aug. 2021].
- [21] J. Belbruno, "Molecularly Imprinted Polymers," *Chem Rev*, vol. 199, no. 1, pp. 94-119, 2018.
- [22] G. Wulff, A. Sarhan and K. Zabrocki, "ChemInform Abstract: ENZYME-ANALOGUE BUILT POLYMERS AND THEIR USE FOR THE RESOLUTION OF RACEMATES," *Chemischer Informationsdienst*, vol. 5, no. 7, 1974.
- [23] Z. El-Schich, "Molecularly imprinted polymers in biological applications," *Biotechniques*, vol. 69, no. 6, pp. 406-419, 2020.
- [24] M. Yan and A. Kapua, "Fabrication of molecularly imprinted polymer microstructures," *Anal Chim Acta*, vol. 345, no. 1, pp. 163-167, 2001.
- [25] R. Boysen, L. Schwarz, S. Li, J. Chowdbury and M. Hearn, "Photo-lithographic patterning of biomimetic molecularly imprinted polymer thin films onto silicon wafers," *Microsyst Technol*, pp. 2037-2043, 20(10-11).
- [26] "Saturation Binding Curves and Scatchard Plots," Graphpad.com, 2021. [Online]. Available: <https://www.graphpad.com/support/faq/prism-3-saturation-binding-curves-and-scatthard-plots/>. [Accessed 13 Aug. 2021].
- [27] A. Dezent, "Multiplexed functionalization of nanoelectromechanical systems with photopatterned molecularly imprinted polymers," *J Micromech Microeng*, vol. 29, no. 2, 2019.
- [28] L. Costa and G. Storti, "Kinetic Modeling of Precipitation and Dispersion Polymerizations," *Polym React Eng*, pp. 45-77, 2017.

- [29] "Acetonitrile," Pubchem.ncbi.nlm.nih, 2021. [Online]. Available: <https://pubchem.ncbi.nlm.nih.gov/compound/acetonitrile>. [Accessed 3 Aug. 2021].
- [30] "Toluene," Pubchem.ncbi.nlm.nih.gov, 2021. [Online]. Available: <https://pubchem.ncbi.nlm.nih.gov/compound/toluene>. [Accessed 16 Aug. 2021].
- [31] "Methyl methacrylate," Pubchem.ncbi.nlm.nih.gov, 2021. [Online]. Available: <https://pubchem.ncbi.nlm.nih.gov/compound/Methyl-methacrylate>. [Accessed 15 Aug. 2021].
- [32] "Divinylbenzene," Pubchem.ncbi.nlm.nih.gov, 2021. [Online]. Available: <https://pubchem.ncbi.nlm.nih.gov/compound/Divinylbenzene>. [Accessed 16 Aug. 2021].
- [33] "(E)-Azobis(isobutyronitrile)," Chemspider, 2021. [Online]. Available: <http://www.chemspider.com/Chemical-Structure.6299.html?rid=75e3b7ff-3cca-4076-b251-9ecc433af5e0>. [Accessed 6 June 2021].
- [34] C. Nguyen, C. Fu, Z. Chen, T. Tran, S. Liu and R. Juang, "Enhanced and selective adsorption of urea and creatinine on amine-functionalized mesoporous silica SBA-15 via hydrogen bonding," *Micropor Mesopor Mat*, vol. 311, 2021.
- [35] M. Włoch and J. Datta, "Synthesis and polymerisation techniques of molecularly imprinted polymers," *Comp Anal Chem*, pp. 17-40, 2019.
- [36] S. N. Prabhu, S. C. Mukhopadhyay, C. P. Gooneratne, A. S. Davidson and G. Liu, "Molecularly Imprinted Polymer-based detection of creatinine," *Med Device Sens*, vol. 3, 2020.
- [37] S. Yu, F. Ng, K. Ma, A. Mon, F. Ng and Y. Ng, "Effect of porogenic solvent on the porous properties of polymer monoliths," *J Appl Polym Sci*, vol. 127, no. 4, pp. 2641-2647, 2012.
- [38] J. Pezzaniti, T. Jeng, L. McDowell and G. Oosta, "Preliminary investigation of near-infrared spectroscopic measurements of urea, creatinine, glucose, protein, and ketone in urine," *Clin Biochem*, vol. 34, no. 3, pp. 239-246, 2001.
- [39] I. Suzuki, "Reagentless Estimation of Urea and Creatinine Concentrations Using Near-Infrared Spectroscopy for Spot Urine Test of Urea-to-Creatinine Ratio," *ABE*, vol. 7, pp. 72-81, 2018.
- [40] B. L. Dunicz, "Simple and accurate method for the determination of creatine and creatinine," *Clin Chim Acta*, vol. 9, no. 3, pp. 203-209, 1964.
- [41] W. Thomas, "1.2: Beer's Law," Libretexts, May 2021. [Online]. Available: [https://chem.libretexts.org/Bookshelves/Analytical_Chemistry/Molecular_and_Atomic_Spectroscopy_\(Wenzel\)/1%3A_General_Background_on_Molecular_Spectroscopy/1.2%3A_Beers_Law](https://chem.libretexts.org/Bookshelves/Analytical_Chemistry/Molecular_and_Atomic_Spectroscopy_(Wenzel)/1%3A_General_Background_on_Molecular_Spectroscopy/1.2%3A_Beers_Law). [Accessed 21 Sept. 2021].
- [42] "Scatchard equation," En.wikipedia.org, 2021. [Online]. Available: https://en.wikipedia.org/wiki/Scatchard_equation. [Accessed 5 Aug. 2021].

- [43] J. Isac-Garcia, J. Dobado, F. Calvo-Flores and H. Martinez-Garcia, "Microscale," *J Chem Educ*, pp. 353-370, 2016.
- [44] S. Miller, "Tips and Tricks for the Lab: Air-Sensitive Techniques (2) :: Education :: ChemistryViews," *Chemistryviews.org*, 2013. [Online]. Available: https://www.chemistryviews.org/details/education/4308331/Tips_and_Tricks_for_the_Lab_Air-Sensitive_Tec. [Accessed 5 Apr. 2021].
- [45] "Sigma-Aldrich vacuum filtration assembly," Millipore Sigma, [Online]. Available: https://www.sigmaaldrich.com/US/en/search/nalgene%C2%AE-filtration-assembly-for-47-mm-filter?focus=products&page=1&perPage=30&sort=relevance&term=Nalgene%C2%AE%20filtration%20assembly%20for%2047%20mm%20filter&type=product_name. [Accessed 4 Oct. 2021].
- [46] Yvon, Jobin, "Horiba," 2020. [Online]. Available: https://static.horiba.com/fileadmin/Horiba/Technology/Measurement_Techniques/Molecular_Spectroscopy/Raman_Spectroscopy/Raman_Academy/Raman_Tutorial/Raman_bands.pdf. [Accessed 25 Oct. 2021].
- [47] G. A. Moss, R. J. Bondar and D. M. Buzzelli, "Kinetic enzymatic method for determining serum creatinine," *Clin Chem*, vol. 21, no. 10, pp. 1422-1426, 1975.

APPENDIX A: NIR SPECTROSCOPY DATA

This section briefly illustrates the inadequacy of the spectroscopy setup for detecting creatinine in the NIR range. Figure 10-1 and Figure 10-2 denote the spectra collected using four samples of creatinine ranging in concentrations between 100 and 1000 mg/dL. Each concentration had 10 samples that were averaged together. A custom MATLAB code, not shown, was used to produce figures. See text for context.

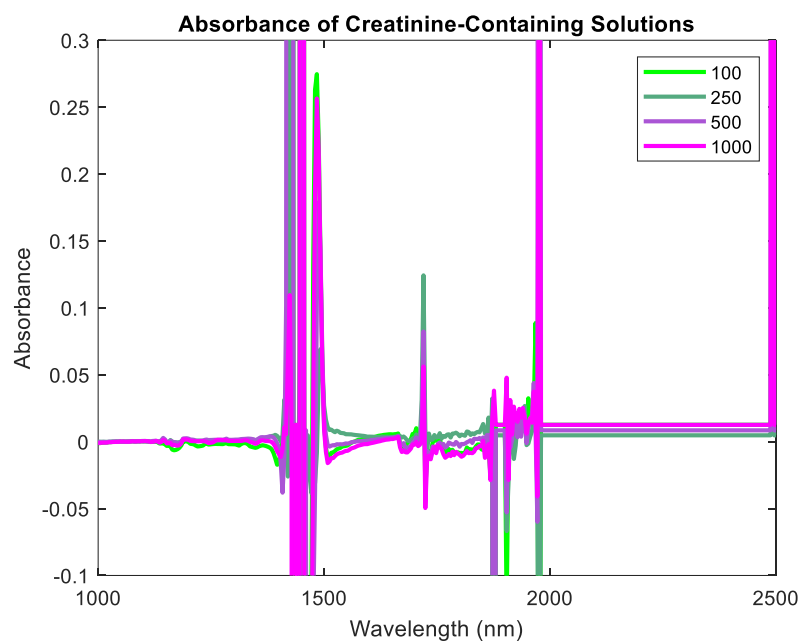


Figure 10-1. NIR spectra for creatinine solutions. Legend depicts concentrations in mg/dL.

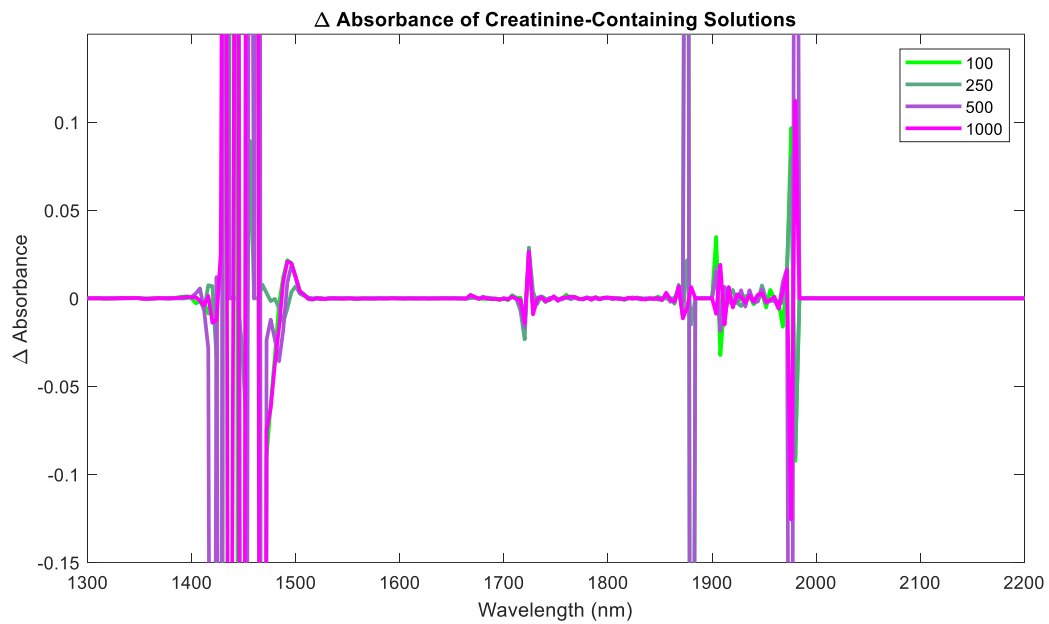


Figure 10-2. Derivative of NIR spectra for creatinine solutions. Legend depicts concentrations in mg/dL.

APPENDIX B: DILUTION SCHEME MATLAB CODE

For convenience, a custom MATLAB code was created in version 2021a that allows for a table containing a basic dilution scheme to be created based on user inputs. The user inputs the concentrations of each dilution stage, alongside the volume of each stage needed (must be consistent). An example output and the source code is provided below.

Table A-2. Example dilution scheme MATLAB code output.

Volume from Prior, mL	Add Solvent, mL	New Concentration, mg/dL	Volume Produced, mL
43 (@ 500 mg/dL)	0	500	43
3	97	15	100
60	30	10	90
50	16.667	7.5	66.667
26.667	13.333	5	40

Dilution scheme source code:

```
%% Bradley Hovan
% RPI Ozisik Lab 2021
%
% Code for calculating basic dilution scheme based on some user
inputs.
%% Inputs
close all; clear; clc
%
% ENTER THESE YOURSELF, THE CODE WILL NOT ASK YOU
Concentrations = [2.5 5 7.5 10 15 20]; % mg/dL, low to high!
Used_Volumes = 20; % mL, how much you need at each concentration.
Spare_Volumes = 0; % mL, how much extra you want.
Output_File = input('Enter file name for output: ','s');
    % ^this will be asked. A text file will be the output, alongside a
    % table in the command window.
%
%% Calculations
Vol_From_Prior = zeros(length(Concentrations),1);
Add_Solvent = zeros(length(Concentrations),1);
Concentrations = flip(Concentrations'); % high to low and turn to
column
Vol_Produced = zeros(length(Concentrations),1);
```

```

    Vol_Needed = Used_Volumes + Spare_Volumes;
    Vol_Produced(end) = Vol_Needed;
% looping for each concentration
for i = length(Concentrations):-1:2
    Dilution_Ratio = Concentrations(i)/Concentrations(i-1);
    Vol_From_Prior(i) = Vol_Produced(i)*Dilution_Ratio;
    Add_Solvent(i) = Vol_Produced(i) - Vol_From_Prior(i);
    Vol_Produced(i-1) = Vol_Needed + Vol_From_Prior(i);
end
Vol_From_Prior(1) = Vol_Produced(1);
% exporting
Dilution_Scheme = table(Vol_From_Prior, Add_Solvent, Concentrations,
Vol_Produced) %#ok<NOPTS>
writetable(Dilution_Scheme, Output_File)
% Creatinine mass needed
mg_Crea = Vol_From_Prior(1)*Concentrations(end)/100;
fprintf('mg creatinine for stock soln: %f mg\n',mg_Crea)

```

APPENDIX C: REFERENCE CURVE MATLAB CODE

This section has two sets of code: the former relating to section 6.1 and the latter relating to section 6.2.

Code for reference curve experimentation:

```
% Reference Curve Script
% Bradley Hovan, Ozisik Lab, RPI
% 09/21/2021
%
%% Inputs
close all; clc; clear
names = dir;
samples = 8; % including H2O samples
cycles = 10;
vars = samples*cycles;
conc = [0, 50, 100, 150, 200, 250, 500, 1000];
rawabs = zeros(14,vars);
wave = table2array(readtable(names(3).name));
wave(:,2) = [];
%
buffer = 2;
for i = buffer+1:1:vars+buffer
    temp = table2array(readtable(names(i).name));
    rawabs(1:length(temp),i-2) = temp(:,2);
    clear temp
end
%
%% Averaging and Averaging Plots
clc
% Averaging
abstemp = zeros(size(rawabs,1),samples);
for i = vars:-cycles:cycles % loop to average cycles
    abstemp(:,i/cycles) = mean(rawabs(:,i-1:i),2); % average cycles
end
abs = abstemp;
% Subtracting H2O
for i = 2:samples
    abs(:,i) = abs(:,i) - abs(:,1);
end
abs(:,1) = []; % updating sample #-dependent variables
samples = samples - 1;
vars = vars - cycles;
conc(1) = [];
% Average Plots (H2O not subtracted)
figure(1)
for i = 1:samples
    subplot(2,4,i)
```

```

    for j = 1:cycles
        plot(wave,rawabs(:,i*cycles+j),'k-','LineWidth',1.5); hold on
    end
    plot(wave,abstemp(:,i+1),'r-','LineWidth',2)
    title(append(string(conc(i)), ' mg/dL, n = 10'))
    xlabel('Wavelength (nm)'); ylabel('Absorbance (AU)')
    axis([265 280 0 4])
    tempstd = std(rawabs(1,i*cycles+1:i*cycles+cycles));
    text(266,3.75,append('*std at 275nm is ',string(tempstd)))
end
% "THE MACHINE IS WORKING"
%
%% Plot Basic Absorbance and Transmittance
clc
% Transmittance
trans = 100./10.^abs;
figure(2)
for i = 1:samples
    colors = [i/(samples-1) - 1/(samples-1), i/(1-samples) -
samples/(1-samples),...
    -i^2/12 + 3*i/4 - 2/3];
    subplot(1,2,1)
    plot(wave,abs(:,i),'LineWidth',2,'Color',colors); hold on
    subplot(1,2,2)
    plot(wave,trans(:,i),'LineWidth',2,'Color',colors); hold on
end
subplot(1,2,1)
xlabel('Wavelength (nm)'); ylabel('Absorbance (AU)')
axis([250 280 0 4]); legend(string(conc))
title('Absorbance at Each Concentration')
subplot(1,2,2)
xlabel('Wavelength (nm)'); ylabel('% Transmittance')
axis([240 280 0 100]); legend(string(conc))
title('% Transmittance at Each Concentration')
%
%% AUC plots
%
clc
limits = [260 280]';
ind = limits;
for i = 1:2*size(limits,2)
    ind(i) = find(wave == limits(i));
end
%
AUC = zeros(2,samples);
for i = 1:samples
    AUC(1,i) = -trapz(wave(ind(2):ind(1)),abs(ind(2):ind(1),i));
    AUC(2,i) = -trapz(wave(ind(2):ind(1)),trans(ind(2):ind(1),i));
end
%
figure(3)
subplot(1,2,1)

```

```

plot(conc,AUC(1,:), 'k--o', 'LineWidth',1.5)
    xlabel('Concentration (mg/dL)'); ylabel('Absorbance*
(AU*\lambda)')
    title(append('Area Under Curve, from ',string(limits(1)), ' to
',...
    string(limits(2)), ' nm'))
subplot(1,2,2)
plot(conc,AUC(2,:), 'k--o', 'LineWidth',1.5)
    xlabel('Concentration (mg/dL)'); ylabel('% Transmittance*')
    title(append('Area Under Curve, from ',string(limits(1)), ' to
',...
    string(limits(2)), ' nm'))
%
%% Absorbance Per-point regression model
% takes each point and correlates it to the conc variable, highest
% correlation wavelength is kept
R2 = 0;
for i = 1:length(wave)
    tempR = corrcoef(abs(i,:),conc);
    tempR2 = tempR(1,2)^2;
    if tempR2 > R2
        R2 = tempR2;
        ind = i;
    end
end
figure(4)
plot(conc,abs(ind,:), 'ko')
xlabel('Concentrations (mg/dL)')
ylabel('Absorbance (AU)')
title(append('Concentration vs Absorbance at ',string(wave(ind)), '
nm'))
legend(append(string(wave(ind)), ' nm'))
%
%% %Transmittance Per-point regression model
% takes each point and correlates it to the conc variable, highest
% correlation wavelength is kept
R2 = 0;
for i = 1:length(wave)
    tempR = corrcoef(trans(i,:),conc);
    tempR2 = tempR(1,2)^2;
    if tempR2 > R2
        R2 = tempR2;
        ind = i;
    end
end
figure(5)
plot(conc,trans(ind,:), 'ko')
xlabel('Concentrations (mg/dL)')
ylabel('% Transmittance')
title(append('Concentration vs % Transmittance at
',string(wave(ind)), ' nm'))
legend(append(string(wave(ind)), ' nm'))

```

Code for reference curve finalization:

```
% Reference Curve Script
% Bradley Hovan, Ozisik Lab, RPI
% 09/24/2021
%
%% Inputs and Boxplots
close all; clc; clear
names = dir;
samples = 7; % including H2O samples
cycles = 20;
vars = samples*cycles;
conc = [2.5 5 7.5 10 15 20];
rawabs = zeros(cycles,samples);
abs = zeros(1,samples-1);
buffer = 2;
for i = 1:samples
    temp = table2array(readtable(names(i+buffer).name));
    rawabs(:,i) = temp(2,2:end);
    clear temp
    if i ~= 1
        rawabs(:,i) = rawabs(:,i) - rawabs(:,1);
        abs(i-1) = mean(rawabs(:,i));
    end
end
rawabs(:,1) = [];
samples = samples - 1;
%
figure(1)
boxplot(rawabs,'Labels',{'2.5','5.0','7.5','10','15','20',})
xlabel('Concentration, not to scale (mg/dL)')
ylabel('\Delta Absorbance')
title('Absorbance Boxplots (n=20)')
%
figure(2)
plot(conc,abs,'ko','MarkerSize',10)
xlabel('Concentration (mg/dL)')
ylabel('\Delta Absorbance')
title('Average Absorbance (n=20)')
```

APPENDIX D: RAMAN SPECTRA MATLAB CODE

Custom MATLAB code used to produce Raman spectra in section 7.

```
% Bradley Hovan
% Raman Samples
% 10/26/2021
%% Inputs
close all; clear; clc
Crea = importdata('BH-Creatinine-10262021.txt');
MIP = importdata('BH-MIP2-10262021.txt');
NIP = importdata('BH-NIP-10262021.txt');
%% Plots
clc
figure(1)
subplot(3,1,1)
plot(Crea(:,1),Crea(:,2),'LineWidth',1.5)
axis([0 4000 600 900])
set(gca,'xdir','reverse')
title('Creatinine Spectrum')
xline(2925.95)
xline(1722.18)
%
subplot(3,1,2)
plot(MIP(:,1),MIP(:,2),'LineWidth',1.5)
axis([0 4000 600 2000])
ylabel('Raman Intensity (a.u.)')
set(gca,'xdir','reverse')
title('MIP Spectrum')
xline(2958.98)
%
subplot(3,1,3)
plot(NIP(:,1),NIP(:,2),'LineWidth',1.5)
axis([0 4000 600 1000])
xlabel('Wavenumber (cm-1)')
set(gca,'xdir','reverse')
title('NIP Spectrum')
xline(2925.95)
xline(1644.13)
```

APPENDIX E: SCATCHARD ANALYSIS MATLAB CODE

Results from this code are not shown due to very poor outcomes. See section 7 for details.

```
% Scatchard Plot Script
% Bradley Hovan, Ozisik Lab, RPI
% 09/29/2021
%
%% Inputs
close all; clear; clc
refH2O = 0.0388; % AU
conc = [5, 7.5, 10, 15, 20]; % mention loss of 2.5 mg/dL samples
ref_abs = [0.00090,0.00215,0.002882,0.004336,0.005485];
% A = 0.000305c - 0.000388
%
samples = 7;
cycles = 30;
vars = samples*cycles;
buffer = 2;
raw_abs_M = zeros(cycles,samples);
raw_abs_N = raw_abs_M;
abs_M = zeros(1,samples);
abs_N = abs_M;
%
names = dir;
for i = 1+buffer:2:samples*2+buffer
    temp = table2array(readtable(names(i).name));
    raw_abs_M(:,(i-1)/2) = temp(2,2:end);
    abs_M((i-1)/2) = mean(temp(2,2:end));
    clear temp
    temp = table2array(readtable(names(i+1).name));
    raw_abs_N(:,(i-1)/2) = temp(2,2:end);
    abs_N((i-1)/2) = mean(temp(2,2:end));
    clear temp
end
%% Boxplot and Ave/std
%
figure(1)
subplot(2,1,1)
boxplot(raw_abs_M,'Labels',{'0: H2O ref','0: MIP
ref','5.0','7.5','10','15','20',})
xlabel('Concentration, not to scale (mg/dL)')
ylabel('Absorbance')
title('MIP Absorbance Boxplots (n=30)')
%
subplot(2,1,2)
boxplot(raw_abs_N,'Labels',{'0: H2O ref','0: NIP
ref','5.0','7.5','10','15','20',})
```

```

xlabel('Concentration, not to scale (mg/dL)')
ylabel('Absorbance')
title('NIP Absorbance Boxplots (n=30)')
%
figure(2)
%
ex_ave = zeros(1,cycles);
ex_std = ex_ave;
for i = 1:cycles
    ex_ave(i) = mean(raw_abs_M(1:i,6));
    ex_std(i) = std(raw_abs_M(1:i,6));
end
yyaxis left
plot(1:30,ex_ave,'b-o','LineWidth',2); hold on
xlabel('Sample number (n)'); ylabel('Average Absorbance (AU)')
axis([0 31 0.0985 0.0995])
yyaxis right
plot(1:30,ex_std,'o-')
ylabel('Standard Deviation of Absorbance')
axis([0 31 0 0.00025])
title('Demonstrating the effect of increased sample size (MIP 15-
mg/dL)')
%% Correcting for H2O / Dissolved contaminants
H2O_M = abs_M(1);
H2O_N = abs_N(1);
dH2O_M = H2O_M - refH2O;
dH2O_N = H2O_N - refH2O;
%
corr_abs_M = abs_M(3:end) - abs_M(2);
%   corr_abs_M = [corr_abs_M(1) corr_abs_M(3) corr_abs_M(2)...
%   corr_abs_M(5) corr_abs_M(4) ];
% corr_abs_N = abs_N(3:end) - abs_N(2);
%   corr_abs_N = [corr_abs_N(1) corr_abs_N(3) corr_abs_N(2)...
%   corr_abs_N(5) corr_abs_N(4) ];
%
% corr2_abs_M = corr_abs_M.*0.09175;
corr2_abs_M = corr_abs_M;
%
figure(3)
plot(conc,corr2_abs_M,'ko')
xlabel('Concentration (mg/dL)')
ylabel('Absorbance (AU)')
% title('Initial concentration versus absorbance, corrected')
% Recall: c =(A + 0.000388)/0.000305
New_conc = (corr2_abs_M + 0.000388)./0.000305; % mg/dL
delta_mg = (conc - New_conc).*0.06; % mg
Q = delta_mg ./ 60; % mg/mg
%
figure(4)
plot(conc,Q,'k-o')
xlabel('Initial Concentration of creatinine (mg/dL)')
ylabel('Q (mg/mg)')

```

```
title('Binding isotherms of creatinine MIP and NIP')
%
Q_crea = Q./conc;
figure(5)
plot(Q,Q_crea,'k-o')
xlabel('Q (mg/mg)')
ylabel('Q/[Crea] (dL/mg)')
title('Scatchard plots of creatinine MIP and NIP')
```

APPENDIX F: SUPPLEMENTARY FILES

F.1 Permissions for section 2.1

This file contains license details and terms and conditions for the reproduction of materials used in Section 2.1 of this dissertation.

File name: Permission_Miura_2013

File type: Portable Document Format (PDF)

File size: 3080 KB

Required application software: Adobe Acrobat or any standard PDF viewer

Special hardware requirement: None

F.2 Permissions for section 3.1

This file contains license details and terms and conditions for the reproduction of materials used in Section 3.1 of this dissertation.

File name: Permission_Belbruno_2019

File type: Portable Document Format (PDF)

File size: 391 KB

Required application software: Adobe Acrobat or any standard PDF viewer

Special hardware requirement: None

This file contains license details and terms and conditions for the reproduction of materials used in Section 3.1 of this dissertation.

File name: Permission_Schich_2020

File type: Portable Document Format (PDF)

File size: 193 KB

Required application software: Adobe Acrobat or any standard PDF viewer

Special hardware requirement: None

This file contains license details and terms and conditions for the reproduction of materials used in Section 3.1 of this dissertation.

File name: Permission_Miura_2013

File type: Portable Document Format (PDF)

File size: 3080 KB

Required application software: Adobe Acrobat or any standard PDF viewer

Special hardware requirement: None

F.3 Permissions for section 3.2

This file contains license details and terms and conditions for the reproduction of materials used in Section 3.2 of this dissertation.

File name: Permission_Prabhu_2020

File type: Portable Document Format (PDF)

File size: 204 KB

Required application software: Adobe Acrobat or any standard PDF viewer

Special hardware requirement: None

This file contains license details and terms and conditions for the reproduction of materials used in Section 3.2 of this dissertation.

File name: Permission_Prabhu_Wiley_2020

File type: Portable Document Format (PDF)

File size: 2101 KB

Required application software: Adobe Acrobat or any standard PDF viewer

Special hardware requirement: None

F.4 Permissions for section 3.3

This file contains license details and terms and conditions for the reproduction of materials used in Section 3.3 of this dissertation.

File name: Permission_Suzuki_2019

File type: Portable Document Format (PDF)

File size: 1644 KB

Required application software: Adobe Acrobat or any standard PDF viewer

Special hardware requirement: None